Journal of Pharmaceutical Sciences 106 (2017) 39-65

Contents lists available at ScienceDirect

Journal of Pharmaceutical Sciences

journal homepage: www.jpharmsci.org

Review

Pharmaceutical Amorphous Nanoparticles

Rajan Jog, Diane J. Burgess*

Department of Pharmaceutical Sciences, University of Connecticut, Storrs, Connecticut 06269

ARTICLE INFO

Article history:
Received 10 August 2016
Revised 6 September 2016
Accepted 15 September 2016
Available online 2 November 2016

Keywords:
amorphous
nanoparticles
nanocrystalline
solubility
stability
dissolution
solid state
calorimetry
X-ray diffraction
bioavailability

ABSTRACT

There has been a tremendous revolution in the field of nanotechnology, resulting in the advent of novel drug delivery systems known as nanomedicines for diagnosis and therapy. One of the applications is nanoparticulate drug delivery systems which are used to improve the solubility and oral bioavailability of poorly soluble compounds. This is particularly important because most of the molecules emerging from the drug discovery pipeline in recent years have problems associated with solubility and bioavailability. There has been considerable focus on nanocrystalline materials; however, amorphous nanoparticles have the advantage of synergistic mechanisms of enhancing dissolution rates (due to their nanosize range and amorphous nature) as well as increasing supersaturation levels (due to their amorphous nature). An example of this technology is Nanomorph™, developed by Soliqus/Abbott, wherein the nanosize drug particles are precipitated in an amorphous form in order to enhance the dissolution rate. This along with other simple and easily scalable manufacturing techniques for amorphous nanoparticles is described. In addition, the mechanisms of formation of amorphous nanoparticles and several physicochemical properties associated with amorphous nanoparticles are critically reviewed.

Introduction

There has been an incredible increase in the identification of potential drug candidates based on the application of high-throughput screening techniques, genomics, combinatorial chemistry, and *in silico* computational approaches.[1-6] Of these potential drug candidates, about 40% do not have "drug-like" properties, such as good aqueous solubility and dissolution rates.[6-9] There are a number of approaches that are utilized to increase the dissolution rate and solubility and thus oral bioavailability of poorly soluble drugs. Traditional approaches to improve drug dissolution rate and solubility include salt formation, use of solubilizing excipients, and complexation agents. However, the success of these traditional approaches has been limited due to the taxing process of selection of highly soluble salts, as well as the requirement for large quantities of solubilizing excipients and complexation agents (http://www.accessdata.fda.gov/drugsatfda_docs/label/2009/020966s022lbl.pdf).

Crystalline or amorphous nanoparticles are an attractive alternative approach to enhance the rate of dissolution and solubility of poorly soluble drugs. Discrete drug particles in the range of 100-1000 nm are defined as pharmaceutical nanoparticles.[10] An increase in the exposed surface area (or surface area-to-volume ratio) by particle size reduction causes an increase in dissolution rate and thus oral bioavailability.[11,12] In addition, according to the Kelvin equation, saturation solubility (in terms of vapor pressure) of the

Abbreviations used: ACN, amorphous chitin nanoparticles; API, active pharmaceutical ingredient; APTES, 3-aminopropyltriethoxysilane; BCS, Biopharmaceutics Classification System; CGN, K-carrageenan; CMC, carboxymethyl cellulose; cps, centipoise; CTAB, cetrimonium bromide; DLS, dynamic light scattering; DMC, dimethyl chitosan; DoE, design of experiment; DS, dextran sulfate; DSC, differential scanning calorimetry; DTAB, dodecyl trimethylammonium bromide; EPL, ε-polylysine; FDA, food and drug administration; FTIR, Fourier transform infrared spectroscopy; GAS, gas antisolvent; HMW, high molecular weight; HPC, hydroxypropyl cellulose; HPβCD, hydroxypropyl β-cyclodextrin; HPMC, hydroxylpropylmethylcellulose; LMW, low molecular weight; MβCD, methyl-β-cyclodextrin; MCC, microcrystalline cellulose; MCM-41, mobile composition of matter no. 41; MMA, methyl methacrylate; MPTMS, (3-mercaptopropyl)trimethoxysilane; NME, nanoporous membrane extrusion; NPs, nanoparticles; O/W, oil in water; PBS, phosphate-buffered saline; PCL, polyε-caprolactone; PEG, polyethylene glycol; PEI, poly(ethylene imine); PLA, polylactic acid; PLGA, poly(lactic-co-glycolic acid); PLM, polarized light microscopy; PM, physical mixture; PSu, propylene succinate; PVA, polyvinyl alcohol; PVP, poly(vinylpyrrolidone); PXRD, powder X-ray diffraction; RESS, rapid expansion of supercritical solutions; RH, relative humidity; SAS, supercritical antisolvent; SAS-EM, supercritical antisolvent enhanced mass transfer; SBA-15, Santa Barbara amorphous type material-15; SCF, supercritical fluid technology; SEM, scanning emission microscopy; SLS, sodium lauryl sulfate; STPP, sodium tripolyphosphate; TEM, transmission emission microscopy; TEOS, tetraethyl orthosilicate; T_g, glass transition temperature; THF, tetrahydrofuran; TMAOH, tetramethylammonium hydroxide; TMC, trimethyl chitosan; TPGS, tocopheryl polyethylene glycol succinate; TPP, pentasodium tripolyphosphate; TRPV1, transient receptor potential cation channel subfamily V member 1; USP, United States Pharmacopeia; W/O/W, water in oil in water; YMCR, Y-junction microchannel reactor.

* Correspondence to: Diane J. Burgess (Telephone: 860-486-3760; Fax: 860-486-2076).

E-mail address: d.burgess@uconn.edu (D.J. Burgess).

http://dx.doi.org/10.1016/j.xphs.2016.09.014
0022-3549/

drug is dependent on the drug particle size (which translates to the curvature effect). Theoretically, reduction in particle size will cause an increase in drug solubility.[13] However, the actual increase in saturation solubility for "nanocrystalline suspensions" (colloidal size range 100-1000 nm) is marginal, approximately 2%-10% compared to unmilled particles. Thus, nanosized crystalline powders may not be a useful approach for solubility-limited drugs (i.e., solubility is rate limiting for oral bioavailability).[14] In the case of amorphous formulations, the solubility of the drug is increased over the crystalline form due to its high energy state (higher Gibbs' free energy).[15-17] However, amorphous formulations are unstable and will convert to the stable crystalline form over pharmaceutically relevant timescales.[18] Generally, amorphous drugs have been formulated as microsized solid dispersions prepared using techniques such as spray drying and hot melt extrusion. For both these techniques, the drug is stabilized in a polymer matrix with a higher glass transition temperature than the neat polymer. Recently, nanosized amorphous formulations, namely "nanoamorphous," have been utilized to enhance the dissolution rates and solubilities of poorly soluble drugs. Theoretically, combining nanotechnology and amorphization approaches may offer absolute or synergistic effects in terms of solubility and dissolution rates. The advantage of amorphous versus crystalline nanoparticles is the considerably higher kinetic solubility of amorphous nanoparticles, which can be as much as 10-fold to 1600-fold. Although a significant amount of research has been carried out on amorphous nanoparticles, there are no marketed drug products available, till date. The major formulation challenge associated with amorphous nanoparticles is their stability, which depends on active pharmaceutical ingredient (API) properties such as the melting temperature (T_m), T_m/T_g ratio, and the properties of the polymer or stabilizer utilized.[19-23] Amorphous systems have higher free volume or enthalpy as well as high Gibbs-free energy. Accordingly, these systems are unstable and tend to crystallize to a stable polymorph of the drug, which typically would have lower solubility. The crystallization time of an amorphous drug is a kinetically controlled process (which can vary from seconds to years) and depends on several factors such as storage temperature and moisture content. Various approaches have been used to stabilize the amorphous form of drugs. For example, crystallization inhibitors (high T_g polymers) can be added and the formulation may be stored at low temperature (50°C below the drug T_g) and low moisture/humidity conditions.[16]

Broadly, there are 2 basic methods to manufacture nanoparticles: (1) a "top-down approach" (i.e., milling/grinding of the particles to achieve the required size) and (2) a "bottom-up approach" (i.e., precipitation of drug from a solvent to an antisolvent system).[11] The top-down approach is very time consuming and usually leads to crystalline particles, whereas the bottom-up approach is less time consuming and usually leads to amorphous particles due to fast evaporation of the solvent and thus precipitation of the API as amorphous particles. The manufacturing techniques employed for amorphous and crystalline nanoparticles are listed in Table 1.

The mechanism by which nanoparticles improve the dissolution rate and bioavailability of poorly water-soluble APIs (Biopharmaceutics Classification System [BCS] Class II and II/IV) is the enhanced surface area to volume ratio as described by the Noyes-Whitney equation.[43] According to the Noyes-Whitney equation, the dissolution rate J is given by the following equation;

$$J = \frac{DA}{h}(C_s - C)$$

where J is the dissolution rate, D the diffusion coefficient of drug, A the surface area of the dissolving solid, h the thickness of the diffusion layer, C_s the saturation solubility of the compound in the dissolution medium, and C the concentration of the drug in the medium at different time points during dissolution.

Increase in the surface-to-volume ratio and thus the dissolution rate of nanoparticles improves their pharmacokinetic properties in terms of increased rate and extent of release and absorption; rapid onset of action; reduced side effects, and improved clinical performance.[11,43,44] Concurrently, the drug saturation solubility is increased as theoretically predicted by the Ostwald-Freundlich equation as below:

$$ln\frac{C_{s,r}}{C_{s,\infty}} = \frac{2\gamma V_m}{rRT}$$

where $C_{s,r}$ and $C_{s,\infty}$ (g/L) are the solubility of drug particles with radii r and $r = \infty$ (m), respectively, c the interfacial tension between the drug particles and the medium (N/m), V_m the drug molar volume (m^3/mol), R the gas constant (8.314 J/mol K), and T the absolute temperature (K).

The importance of crystalline nanosuspensions to the pharmaceutical industry can be judged by the fact that 17 formulations are already on the market and approximately 10-15 are in different stages of clinical trials (Tables 2 and 3).[34] However, one of the major concerns with nanosuspension formulations is the preservation of their physical and chemical stability in aqueous medium.[51,52] Experimental and computational approaches to estimate solubility and permeability in drug discovery and development settings being a liquid dosage form, nanosuspensions are more susceptible to both physical instability (due to crystal growth and agglomeration) and chemical instability (due to degradation of the API(s)), when compared to solid dosage forms. In fact, of all the marketed formulations, only Megace ES is in the suspension form (nanoparticulate suspension of megestrol acetate). All others are prepared as nanosuspension-based solid dosage forms, as a way to overcome instability problems. Liquid nanosuspensions can be converted into solid dosage forms by drying to obtain a powder of nanosized drug particles, which can be processed into conventional dosage forms such as tablets or capsules. Spray and freeze drying are the most common methods of removing water from aqueous systems.[51,52]

Terminologies in Solid-State Pharmaceuticals

Solid Solution

If the API is molecularly dissolved in the solid excipient matrix, it is termed a solid solution. In crystalline solid solutions, the API can occupy crystal lattice sites or the interstitial spaces. If the formulation is amorphous, such as when the API is dispersed in an amorphous polymer, the API is distributed at random between the excipient molecules, and can be present as amorphous particles or in molecular solution.[53]

Solid Dispersion

If the API is dispersed as crystalline or amorphous particles in the solid excipient matrix, it is termed a solid dispersion. The matrix may be either a small molecule or a polymer. The dispersed state may include many forms such as eutectic mixtures, crystalline/glass solutions, and amorphous/crystalline suspensions.[53]

Amorphous Solid Dispersions

Amorphous solid dispersions are dispersions of amorphous drug, which is in the molecularly dispersed state (i.e., as a glass solution) in the amorphous polymer matrix.[45]

Table 1
Array of Manufacturing Techniques (Crystalline and Amorphous Nanoparticles)

Technology	Company/Research Group	Pros	Cons	Reference
Bottom-up approach				
Hydrosol, Nanomorph™ (solvent-antisolvent precipitation technique)	Sandoz-Novartis, Abbott/Soliqs	Simple, economically feasible, and easy to scale up	Crystal growth affecting bioavailability	24
Supercritical fluid process (RESS and SAS)	G.W. Pace et al.	Rapid decrease in the pressure of a supercritical fluid in which the lipophilic drug is dissolved	Solubility of the drug in the solvent	25,26
Spray drying (Nano spray dryer B90)	Buchi Corporation	Produces dry material of controllable particle size, shape, form, and moisture content	High installation cost, low thermal efficiency, product recovery	27
Electrospraying	Xie and Zhang et al.	Produces small and uniform particle size, operation parameters easy to control, easy to scale up	Macromolecule degradation due to the thermal/shear stress involved in the operation parameters	28,29
Top-down approach				
Microfluidization, Insoluble Drug Delivery—Particles™	Skye Pharma Canada, Inc.	Sufficient shear to produce nanocrystals	50-100 passes required through the microfluidizer, resulting in an increase in microsized particles in addition to nanoparticles	30,31
High pressure homogenization (piston-gap), DissoCubes®	Skye Pharma, formerly Drug Delivery Services GmbH	Jet milling of drug dispersion in a surfactant medium followed by high pressure homogenization (nanosuspension in water at room temperature)	Hydrolysis of water-sensitive drugs and problems during subsequent drying steps, requires expensive drying techniques such lyophilization	32,33
High pressure homogenization (piston-gap), Nanopure®	PharmaSol GmbH, Berlin	Dispersion media with a low vapor pressure, homogenization at low temperature (nanosuspension in nonaqueous media)	Residual solvent difficult to remove	34,35
Pearl/Ball milling	Liversidge and coworkers	Produces homogenous amorphous preparation of poorly soluble drugs	Potential contamination of the product by erosion of the milling material, relatively long milling times for hard crystalline drugs, and limited scaling up due to the weight of large-scale pearl mills	36,37
Media milling, Nanocrystals®	Elan® drug technologies	Reproducible, cost-effective, and control over drug particle size	Potential contamination of the final product with milling media or machine parts as a result of erosion during milling	12,38
Combination technologies				
Nanoedge™ (bottom up + top down) a. Nanoedge (microprecipitation + HPH) b. H69 (microprecipitation immediately followed by HPH) c. H42 (drug pretreatment by spray drying + HPH) d. H96 (freeze drying + HPH) e. Combinative technology (media milling + HPH)	Baxter	1. Precipitation 2. High pressure homogenization 3. Annealing converting the amorphous particles into partially amorphous or crystalline particles This maintains the drug stability during product shelf life	Expensive and complicated process, residual organic solvent difficult to remove	39,40
Microfluidization reaction technology (bottom up + bottom down)	Gruverman and coworkers	Produces uniform and optimally sized nanoparticles, cost-effective	Expensive and complicated	41,42

HPH, high pressure homogenization.

Table 2
FDA Approved Amorphous Solid Dispersions[45-47]

No.	Drug	Polymer	Trade Name	Drug T_m (°C)	Manufacturer	Manufacturing Technique	Dosage Form	Year
1	Etravirine	HPMC	Intelence®	265	Janssen	Spray drying	Tablet	2008
2	Everolimus	HPMC	Zortress®	115	Novartis	Spray drying	Tablet	2010
3	Fenofibrate	PEG/Poloxamer	Fenoglide®	81	Sanarus, Inc.	Melt granulation	Tablet	2007
4	Itraconazole	HPMC	Sporanox®	166	Janssen	Fluid-bed bead layering	Capsule	1992
5	Itraconazole	HPMC	Onmel®	166	Stiefel	Hot melt extrusion	Tablet	2010
6	Ivacaftor	HPMCAS	Kalydeco®	291	Vertex	Spray drying	Tablet	2012
7	Lopinavir/Ritonavir	PVP-VA64	Kaletra®	125/122	Abbott	Hot melt extrusion	Tablet	2007
8	Nabilone	PVP	Cesamet®	160	Valeant	Solvent evaporation	Tablet	1985
9	Nimodipine	PEG	Nimotop®	125	Bayer	–	Capsule	2006
10	Nivaldipine	HPMC	Nivadil®	147	Fujisawa	–	Tablet	1989
11	Ritonavir	PVP-VA64	Norvir®	122	Abbott	Hot melt extrusion	Tablet	2010
12	Tacrolimus	HPMC	Prograf®	128	Fujisawa	Solvent evaporation	Capsule	1994
13	Telaprevir	HPMCAS	Incivek®	246	Vertex	Spray drying	Tablet	2011
14	Vemurafenib	HPMCAS	Zelboraf®	272	Roche	Solvent-controlled precipitation	Tablet	2011
15	Verapamil	HPC/HPMC	Isoptin® ER-E	<25	Abbott	Hot melt extrusion	Tablet	1981
16	Griseofulvin	PEG	Gris-PEG™	220	Valeant	Hot melt extrusion	Tablet	2000
17	Rosuvastatin	HPMC	Crestor®	151	IPR	Spray drying	Tablet	2002
18	Duloxetine	HPMCAS	Cymbalta®	162	Lilly	–	Capsule	2004
19	Tolvaptan	–	Samsca®	226	Otsuka	Granulation	Tablet	2009
20	Posaconazole	HPMCAS	Noxafil®	170	Merck/Schering	Melt extrusion	Tablet/oral suspension	2013
21	Dasabuvir/Ombitasvir/ Paritaprevir/Ritonavir(R)	PVP-VA/TPGS	Viekira™	120 (R)	AbbVie	Melt extrusion	Tablet	2014
22	Lumacaftor/Ivacaftor(I)	HPMCAS/SLS	Orkambi®	291 (I)	Vertex	Spray drying	Tablet	2015

FDA, US Food and Drug Administration; HPC, hydroxypropyl cellulose; HPMCAS, hydroxypropyl methylcellulose acetate succinate; TPGS, tocopheryl polyethylene glycol succinate.

Amorphous Nanoparticles

Amorphous drug nanoparticles are solid dispersions of submicron colloidal dispersions of discrete drug particles, ranging from 100 to 1000 nm, stabilized with polymers, surfactants, or a mixture of both polymer and surfactant, which has a disordered arrangement.[10,54]

Origin of Pharmaceutical Amorphous Nanoparticles

Amorphous drug nanoparticles were first prepared using HYDROSOL technology (bottom-up to precipitation process) developed by Sucker and coworkers (Sandoz-Novartis), the marketed drug product is called "Nanomorph™" (Abbott/Soliqs, formerly BASF/Knoll). Briefly, the poorly soluble BCS Class II and II/IV drugs are dissolved in suitable organic solvents, this drug stock solution is rapidly added to a nonsolvent (mainly water containing surfactant), resulting in the formation of a supersaturated drug solution and submicron amorphous drug particles are produced.[55]

Properties of Amorphous Nanoparticles

In addition to their nanosize range, amorphous nanoparticles have short-range order, because the molecules are randomly oriented in a variety of conformational states compared to crystalline drugs (which are characterized by long-range order in a compact crystal lattice arrangements; Fig. 1).[56] Amorphous nanoparticles have liquid-like properties at the molecular level, but solid-like properties at the macroscopic level. Heat content or changes in molar volume (Y) with changes in temperature (X) are the important characteristics defining the behavior of amorphous drugs. In the plot of Y versus X, for amorphous drugs, a temperature transition is observed, above which the material is in the rubbery state and below which the material is in the glassy state. This is called the glass transition temperature (T_g), which is an important event for amorphous drugs.

In case of amorphous drugs, the sharp diffraction peaks under powder X-ray diffraction (PXRD) (characteristic of crystalline drugs) are absent; instead, a halo pattern is observed for the amorphous drugs. The glass transition temperature and lack of birefringence is a characteristic of amorphous drugs, which is observed in differential scanning calorimetry (DSC) and polarized light microscopy (PLM), respectively.

Preparation of Amorphous Nanoparticles

Currently, amorphous drugs are formulated in the form of solid dispersions, which are in the micron size range, using different techniques such as spray drying, freeze drying, or hot melt extrusion. Here, drug stability is assured by the addition of high glass transition (T_g) polymers such as HPMC (hydroxylpropylmethylcellulose) and PVP [poly(vinylpyrrolidone)]. The advantages of using these polymers are they minimize the molecular motion of the dispersed drug and hence (1) prevent solution-facilitated crystal growth and nucleation of the dissolved drug, maintaining the supersaturation level for a long period of time and (2) improve the storage stability by inhibiting the recrystallization of amorphous drug. Stabilization of amorphous drug nanoparticles can be achieved by the presence of stabilizers such as polymers, surfactants, and sugars. These excipients are adsorbed on the surface of the nanoparticles via electrostatic or hydrophobic interactions. Excipient adsorption occurs instantaneously following the production of amorphous nanoparticles, inhibiting recrystallization of the high energy sites on the particles, as well as preventing particle growth due to Ostwald ripening.[20] Various techniques have been used to prepare amorphous nanoparticles, such as ultrasonication, drug-polyelectrolyte complexation, anti-solvent precipitation, solvent evaporation, sonoprecipitation, flash nanoprecipitation, and nanoporous membrane extrusion (NME).[57-74] Each of these preparation processes is described in brief in this review. Extensive research has been carried out to study the effect of different types of stabilizers on the stability, *in vitro* dissolution rates, and *in vivo* bioavailability of amorphous drugs, in the micron and nanosize range.[57-75] A higher amount of stabilizer in amorphous nanoparticulate delivery systems confirms greater stability of the amorphous state; however, the dissolution rate may no longer depend on the amorphous nanoparticles, but also on the

Table 3
FDA Approved Nanocrystals[48-50]

No.	Drug	Polymer	Trade Name	Drug T_m (°C)	Manufacturer	Manufacturing Technique	Dosage Form	Year
1	Aprepitant	MCC/HPC	Emend®	255	Merck	Wet ball milling	Capsule	2003
2	Brinzolamide	Carbomer 974P	Azopt®	131	Alcon	Wet ball milling	Suspension	1998
3	Dexmethylphenidate hydrochloride	Ammonio methacrylate copolymer, methacrylic acid copolymer, PEG	Focalin XR®	218	Novartis	Wet ball milling	Capsule	2001
4	Diltiazem	HPC/HPMC	Herbesser®	187	Mitsubishi	Wet ball milling	Tablet	2002
5	Fenofibrate	Hypromellose 2910	Tricor®	81	Abbott	Wet ball milling	Tablet	2004
6	Fenofibrate	Crosspovidone/CMC Na	Triglide®	81	Skye Pharma	Wet ball milling/high pressure homogenization	Tablet	2005
7	Griseofulvin	MC/PEG 400/PEG 8000	Gris-Peg®	220	Novartis	Precipitation	Tablet	1982
8	Megestrol acetate	HPMC	Megace® ES	218	Par Pharma	Wet ball milling	Suspension	2005
9	Methylphenidate hydrochloride	Ammonio methacrylate copolymer, methacrylic acid copolymer, PEG	Ritalin LA®	224	Novartis	Wet ball milling	Capsule	2002
10	Morphine sulfate	Ammonio methacrylate copolymers, Povidone USP	Avinza®	250	King Pharma	Wet ball milling	Capsule	2002
11	Nabilone	Povidone	Cesamet®	155	Lilly	Precipitation	Capsule	2005
12	Naproxen sodium	Ammonio methacrylate copolymer Type A, ammonio methacrylate copolymer Type B, povidone, crospovidone, MCC	Naprelan®	155	Wyeth	Wet ball milling	Tablet	2006
13	Paliperidone palmitate	PEG 4000	Invega Sustenna®	180	Johnson & Johnson	Wet ball milling/high pressure homogenization	I.M. injection	2009
14	Sirolimus	Phosphatidylcholine, propylene glycol	Rapamune®	184	Wyeth	Wet ball milling	Tablet	2000
15	Theophylline	Ethyl cellulose, HPC, povidone	Theodur®	273	Mitsubishi Tanabe Pharma	Wet ball milling	Tablet, capsule	2008
16	Tizanidine hydrochloride	MCC	Zanaflex®	280	Acorda	Wet ball milling	Capsule	2002
17	Verapamil hydrochloride	Povidone	Verelan PM®	131	Schwarz Pharma	Wet ball milling	Capsule	1998

CMC, carboxymethyl cellulose; FDA, US Food and Drug Administration; HPC, hydroxypropyl cellulose; MCC, microcrystalline cellulose; USP, United States Pharmacopeia.

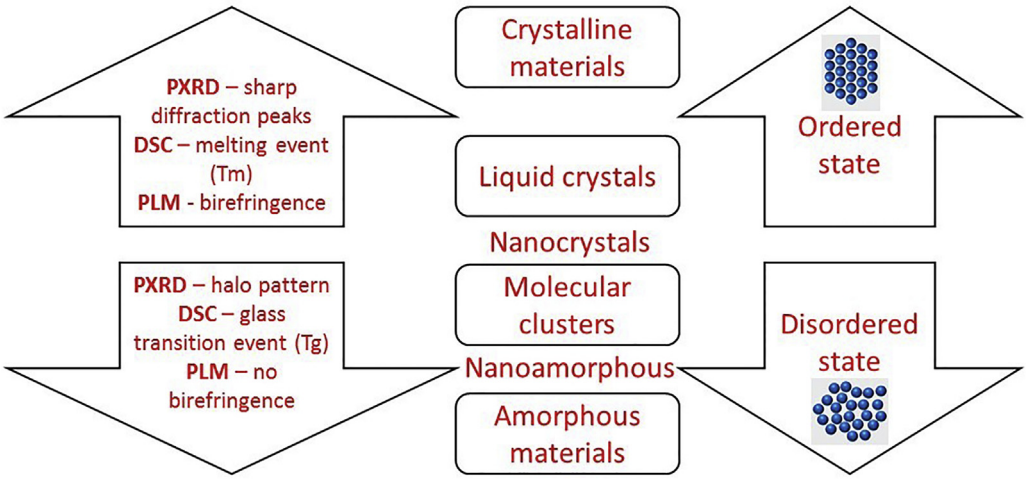

Figure 1. Pictorial representation of different solid-state forms with important solid-state characterization techniques. The ordered arrangement (crystals) is in the top portion and the disordered arrangement (amorphous) is in the bottom portion. Reproduced with permission from Bellantone.[56]

nature of the excipient. Furthermore, a lower content of excipient may not have a significant effect on the dissolution rate, but the formulation may be subject to the risk of recrystallization, affecting the storage stability of the amorphous nanoparticles. Thus, it is necessary to incorporate a suitable concentration of the stabilizer, which is sufficient to improve the storage stability, but yet has a minimal effect on the dissolution rate for the amorphous nanoparticles.[12]

Methods of Manufacturing Amorphous Nanoparticles

Ultrasonication

Ultrasonication is an important top-down processing method for preparation of nanosize drugs. The generation of crystalline or amorphous nanoparticles depends on the intensity, time of exposure, type and concentration of stabilizer used, and type of drug molecule. Ultrasonication improves the mixing of the precursors and increases mass transfer at the particle surface. This leads to smaller particle size and higher size uniformity.[57]

Mechanism Involved

In ultrasonication, high and low pressure phases are generated due to the propagation of acoustic pressure waves in the liquid medium. Cavities are created due to the low pressure phase (which is below the saturation vapor pressure of solution). These cavities absorb energy and grow until unstable when they finally collapse violently generating shock waves in the liquid medium. There is interaction between the particles and the shock waves as a result of the localized high temperature and pressure regions created as a result of the implosions of these cavities. Hence, there is fragmentation of matter due to such extreme conditions resulting in the generation of amorphous nanoparticles. These nanoparticles can be spray or freeze dried to obtain dry amorphous nanoparticles.[67]

Drug-Polyelectrolyte Complexation

In this method, the drug component is mostly an amphiphilic molecule and the complexes are formed due to the simultaneous electrostatic and hydrophobic interactions between the polyelectrolyte and the ionized amphiphile resulting in various structures depending on the nature of the amphiphile.[61,62]

Mechanism Involved

Anionic or cationic drug solute is obtained by dissolving a sparingly soluble amphiphilic molecule in acidic or basic medium. Consequently, an oppositely charged polyelectrolyte solution is added into the ionized drug solution, instigating drug-polyelectrolyte electrostatic interaction and concomitant charge neutralization. There is a rapid loss of solubility resulting in instantaneous precipitation when the drug solute is converted back to its sparingly soluble form upon charge neutralization. As a result, drug-polyelectrolyte nanocomplexes are generated. The synergistic effects of strong electrostatic interactions and rapid precipitation between the drug and polyelectrolyte prevent the drug molecules from arranging into an ordered crystal lattice, resulting in the formation of drug-polyelectrolyte amorphous nanoparticles (Fig. 2).[58]

Antisolvent Precipitation

One of the bottom-up nanosizing techniques for the preparation of amorphous nanoparticles is antisolvent precipitation/crystallization technique. This method has been used extensively as a strategy to enhance the dissolution of poorly soluble drugs. It is a simple technique, cost effective, and easy to scale up.[70]

Mechanism Involved

The drug is dissolved in a known solvent and the excipients are dissolved in an antisolvent. The drug solution is added to the antisolvent containing the stabilizers under controlled stirring, resulting in drug precipitation. Drug precipitation is controlled by the presence of stabilizers in the antisolvent, which inhibit crystallization, decrease the nucleation rate, and enhance the formation of a disordered amorphous solid-state form. Antisolvent precipitation may be conducted in conjunction with sonication. Sonication significantly increases the nucleation rate and hence there is insufficient time to form stable crystal lattices.[73]

Solvent Evaporation

Solvent evaporation is a popular, relatively straight forward and efficient encapsulation method for many hydrophobic drugs.

Mechanism Involved

Solvent evaporation is based on the emulsification of an organic solvent containing polymer in an aqueous phase, following

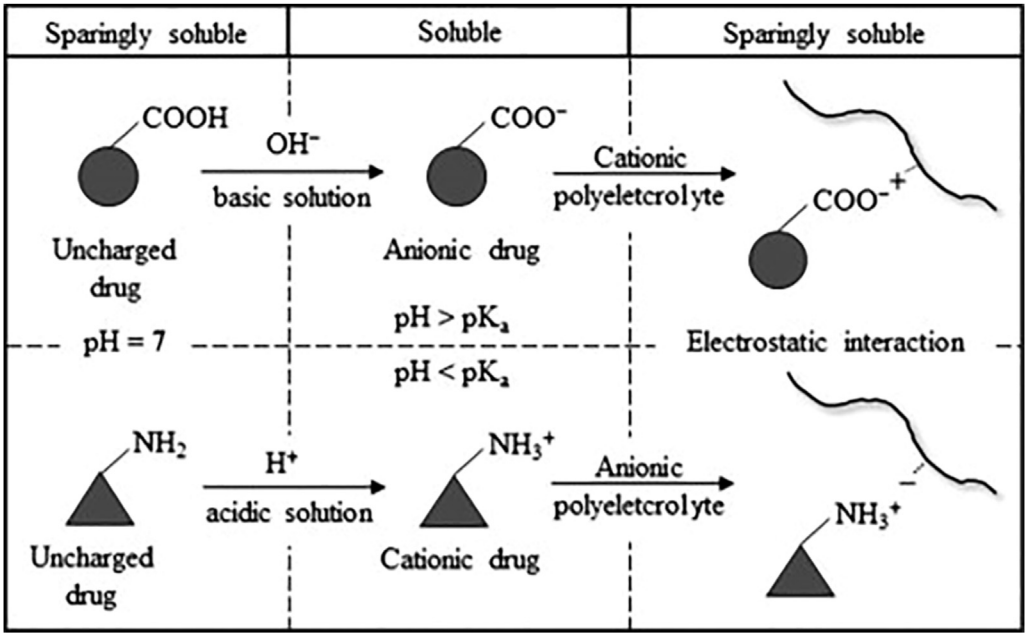

Figure 2. Electrostatic interaction between oppositely charged drugs and polyelectrolytes resulting in drug precipitation (carboxyl and amino groups are used as representative groups of anionic and cationic drugs). Reproduced with permission from Thunemann.[58]

evaporation of the organic solvent, the polymer precipitates in the form nanoparticles. The emulsion droplets which are stabilized by surfactants shrink, but remain relatively stable during solvent evaporation, and these initial emulsion droplets are the basis for the formation of the nanoparticles. Additionally, some emulsion droplets may coalesce during solvent evaporation generating nanoparticles, the size of which is based on the aggregation ratio.[59]

Sonoprecipitation

Sonoprecipitation is the application of ultrasound during antisolvent precipitation to produce discreet, nonagglomerated, and amorphous nanoparticles to enhance the oral bioavailability of hydrophobic drugs. Poor micromixing during antisolvent precipitation leads to uneven supersaturation regions and particle aggregation. Ultrasound in conjunction with antisolvent precipitation provides uniform mixing conditions throughout the vessel.

Mechanism Involved

When ultrasound is propagated through a liquid medium, it increases mass transfer and initiates cavitation. The cavitation bubbles formed during the negative pressure phase of the sound waves implode, creating localized hot spots with a high temperature and pressure, releasing powerful shock waves. Ultrasound results in homogenous mixing of the solvent and antisolvent. The solubility of the solute decreases, instantaneously achieving maximum supersaturation, causing rapid induction of primary nucleation, decrease in crystal size, and prevention of aggregation.[63]

Advanced Methods

Flash Nanoprecipitation

Flash nanoprecipitation is a relatively fast, simple, scalable process using rapid micromixing to create high supersaturation conditions leading to the precipitation and encapsulation of hydrophobic drugs in a polymer-based delivery vehicle.

Mechanism Involved. A mixture of an amphiphilic block copolymer along with a highly hydrophobic drug is dissolved in a water miscible organic solvent. This solution is injected into a small chamber at a high velocity along with water; this high velocity produces a turbulent mixing effect resulting in precipitation of the hydrophobic drug and polymer instantaneously, leading to the formation of nanosize range particles. Amphiphilic block copolymers consist of hydrophobic and hydrophilic regions. The hydrophobic region of the polymer and drug is encapsulated in the core of the nanoparticle. The hydrophilic region forms a corona, sterically stabilizing the particles and preventing further aggregation. The hydrophilic regions can be tipped with ligands for specific cell targeting. The flash nanoprecipitation uses a 4-stream multi inlet vortex mixer or a 2-stream confined impingement jet mixer with subsequent dilution (Fig. 3).[66]

Nanoporous Membrane Extrusion

NME is a novel, simple, low-cost, and efficient technique to prepare uniform 100-nm hydrophobic drug nanoparticles. It is applicable to a wide class of poorly water-soluble drugs and the resulting nanoparticles enhance drug solubility.

Mechanism Involved. The nanoparticles are prepared by pumping one liquid containing hydrophobic drug dissolved in a suitable organic solvent into the other liquid containing a buffer solution, through a nanoporous membrane. Membranes with uniform and well-defined nanopores are essential for the preparation of nanoparticles with reduced sizes (Fig. 4).[69]

Supercritical Fluid Technology

Supercritical fluids (SCFs) are substances that have properties in between that of a gas and liquid (they exists as a vapor and liquid in equilibrium at high temperature and pressure). Substances have superior solubility in the liquid state compared to the gaseous state. The density of substances in the supercritical state is close to that of the same substances in the liquid state. In addition, the diffusivity and viscosity of substances in the supercritical state is close to that

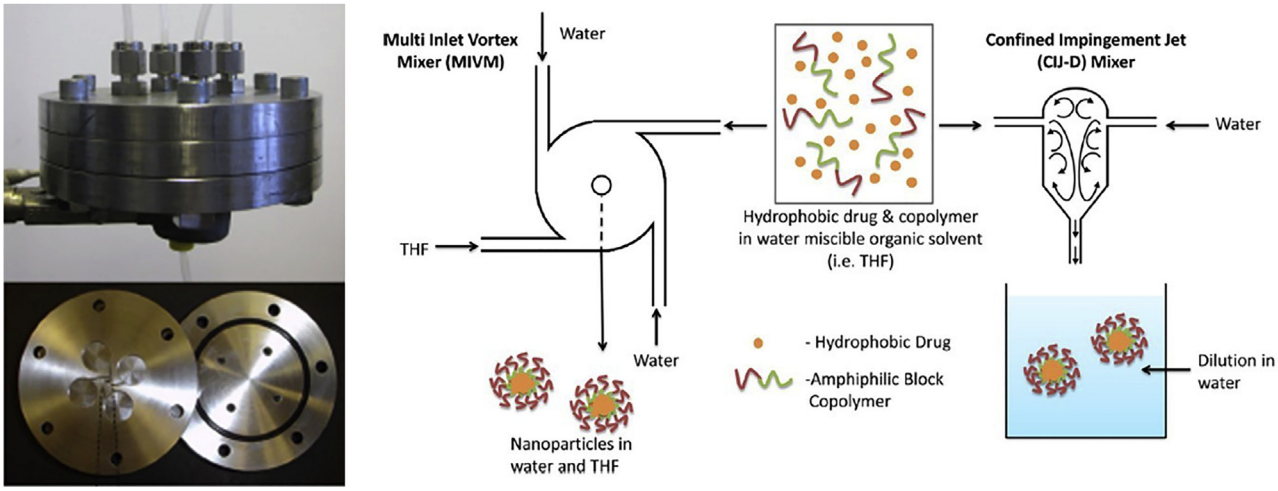

Figure 3. (Left) Assembly of multi inlet vortex mixer. (Right) Schematic diagram of a 4-stream multi inlet vortex mixer and a 2-stream confined impingement jet mixer. Reproduced with permission from Zhu et al.[66]

of the same substances in gaseous state (providing superior mass transfer rates in the SCF state).[76,77] There are 6 SCF technologies: (1) rapid expansion of supercritical solutions (RESS); (2) supercritical antisolvent (SAS); (3) gas antisolvent (GAS); (4) solution enhanced dispersion by SCFs; (5) particle from a gas saturated solution; and (6) carbon dioxide—assisted nebulization with a bubble dryer®. The techniques (a)-(c) mainly produce amorphous nanoparticles, while the techniques (d) and (e) produce amorphous/crystalline microparticles.[78,79]

Mechanisms Involved

Rapid Expansion of Supercritical Solutions. The principal criteria for the application of this technique are that the drug must be freely soluble in the SCF (e.g., supercritical CO_2). The SCF is saturated with neat drug or a drug-polymer mixture. This solution is passed under decompression through a hot nozzle which results in sudden expansion of the mixture leading to rapid nucleation and formation of nanoparticles, collected from the gas stream (Fig. 5).[76,77,80]

Supercritical Antisolvent. Drug or a drug-polymer mixture is dissolved in the organic solvent and this mixture is sprayed through a hot nozzle in a chamber containing SCF, which acts as an antisolvent. There is a large volumetric expansion and consequent density drop as a result of solubilization of the SCF in the organic solvent droplets. This results in increased supersaturation of the solution leading to the formation of uniform-sized nanoparticles (Fig. 6).[76,77,80]

Gas Antisolvent. Drug or a drug-polymer mixture is dissolved in an organic solvent or a mixture of organic solvents. A gas (need not be supercritical) is injected in the solution from the bottom of a closed unit. The gas must be readily soluble in organic solvent, while the drug solubility must be minimal in the gas. The low drug solubility results into supersaturation leading to rapid precipitation and formation of nanoparticles (Fig. 7).[76,77,80]

Mesoporous Silica

Tetraethyl orthosilicate (TEOS) is mixed with alcohol, ammonia, and water to form nanoparticles. The particle size of the nanoparticles is optimized by controlling the ratio of solvent/TEOS. Further agitation and heating lead to pore formation resulting in hollow mesoporous silica nanoparticles. Drug loading is carried out using one of the reported methods: adsorption from organic solution, incipient wetness impregnation technique, melt method, and SCF processing method. Mostly, the solid state of the drug in the mesoporous nanoparticles is amorphous (Fig. 8).[81-86]

Electrospinning

A high voltage is applied to a drug, drug-polymer solution, or melt resulting in an electrically charged jet stream. A Taylor cone-like structure is formed as the voltage is increased, which is due to elongation of the crescent surface of the drug-polymer solution or melt at the tip of the capillary. The solvent evaporates and the

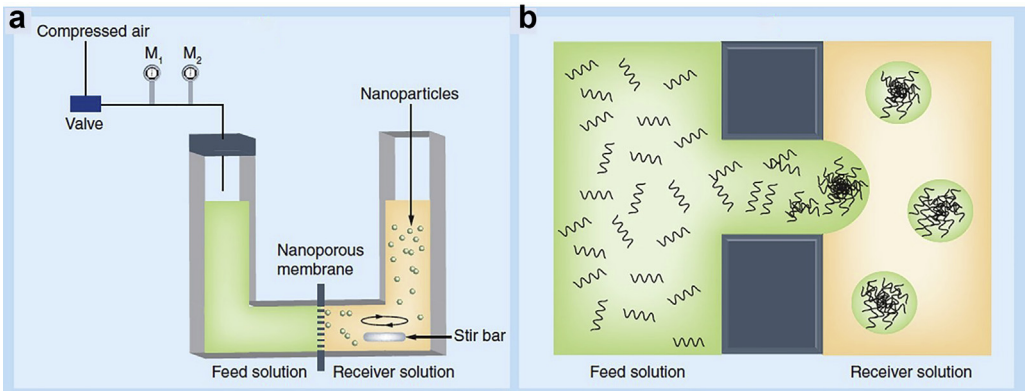

Figure 4. (a) Experimental setup: M1 = pressure meter; M2 = flow meter and (b) formation of nanoparticles in the reservoir. Reproduced with permission from Guo et al.[69]

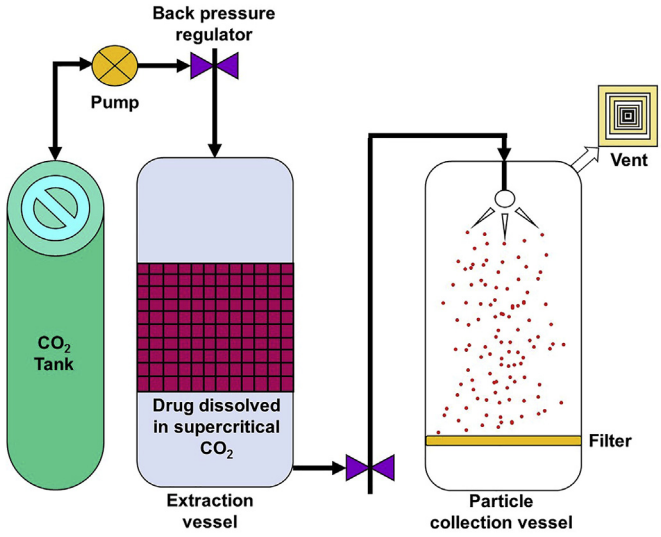

Figure 5. Schematic diagram describing particle formation in RESS equipment.

mixture solidifies, which is collected in a screen as interconnected nanofibers (Fig. 9).[87-91]

Evaluation of Amorphous Nanoparticles

Ultrasonication

Case Study

(1) Wijesena et al. described a top-down preparation process for chitosan nanoparticles and nanofibers using direct ultrasonication (Fig. 10). Chitin nanofibers, with a diameter of 5 nm, were prepared using ultrasonication. An ultrasound tip operating at a frequency and power of 24 kHz and 360 W both for 15 min, respectively, was used for ultrasonication. These nanofibers were used as a precursor for the preparation of amorphous chitosan nanoparticles, with diameters <300 nm as determined using atomic force microscopy and halo pattern PXRD.

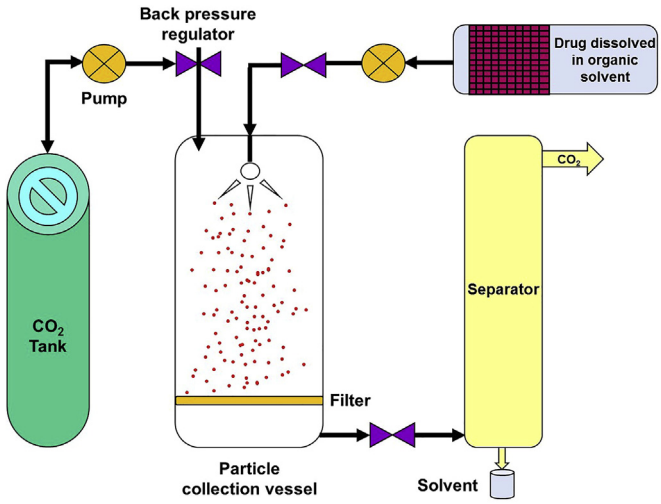

Figure 6. Schematic diagram describing particle formation in the SAS process.

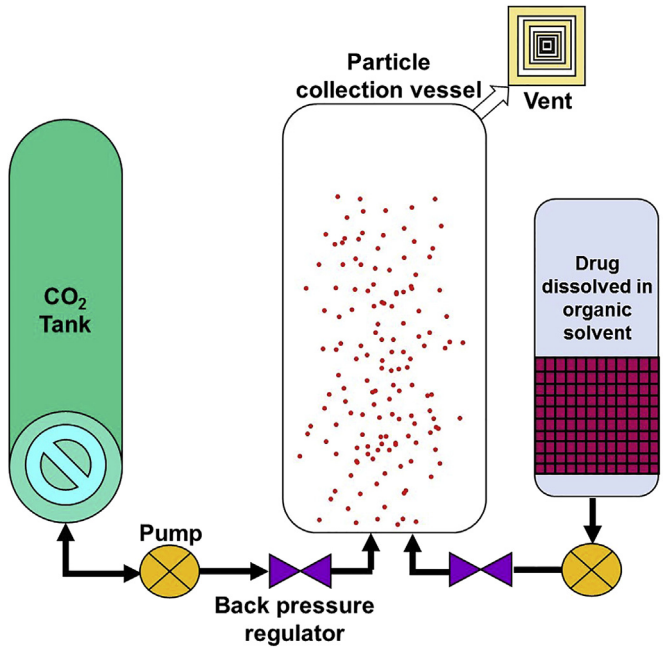

Figure 7. Schematic diagram describing particle formation in the GAS process.

Transmission electron microscopy (TEM) images show that the actual size of the chitosan nanoparticles was 100 nm. Due to the cavitation effect, the chitin nanofibers were fragmented into tiny seed particles (25 nm), which self-assembled to form larger chitosan nanoparticles (<300 nm). Further ultrasonication of nanofibers can result in scission and fragmentation resulting in smaller sizes. These phenomena are observed in carbon nanotubes and some polymer nanofibers.[74]

Drug-Polyelectrolyte Complexation

Case Studies

(1) Cheow et al. prepared self-assembled drug-polyelectrolyte amorphous nanoparticle complexes, demonstrating enhanced dissolution rate and saturation solubility. Two aqueous salt solutions, one containing drug (ciprofloxacin) and the other containing oppositely charged polyelectrolyte (dextran sulfate), were mixed to prepare the amorphous nanoparticle complex also named as a nanoplex. Freeze drying was used to convert the nanoplex suspension into a stable, dry powder (Fig. 11).

Electrostatic and hydrophobic interactions between ciprofloxacin-dextran and ciprofloxacin-ciprofloxacin, respectively, are responsible for maintaining the nanoplex structure. The presence of salt has a significant role in the self-assembly of ciprofloxacin nanoplexes due to the electrostatic charge shielding function of the salt. The charge shielding enables the dextran chains to come in close contact with each other and similarly ciprofloxacin chains come in close contact leading to the formation of core-shell ciprofloxacin nanoplexes, which precipitate.

The amorphous nanoplex morphology was determined to be nearly spherical with a particle size range of 200-400 nm under field emission scanning electron microscopy and a drug loading of 80%. The drug concentration and drug:salt concentration determine the complexation efficiency. The amorphous nature of the nanoplex was proven under PXRD, which displayed a halo pattern.

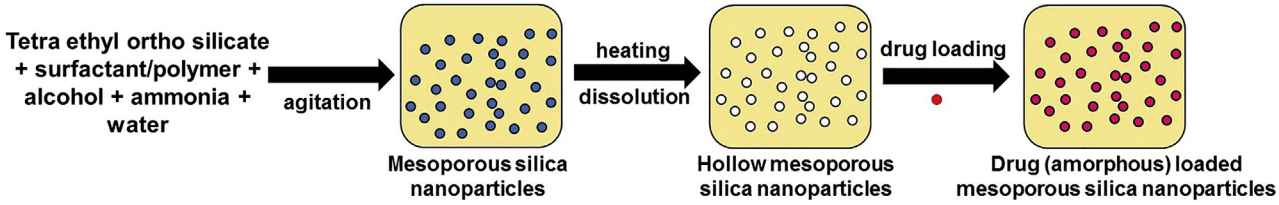

Figure 8. Preparation of a mesoporous silica nanoamorphous formulation.

The dissolution rate and solubility were approximately double for the nanoplex powder compared to the crystalline drug. Under storage stability at 25°C/55% RH (relative humidity), the powder was determined to be stable after 1 month. The advantages of the drug-polyelectrolyte amorphous nanoplex system are the following: (1) faster dissolution rate due to the nanosize and amorphous solid-state form; (2) higher supersaturation level compared to the crystalline drug; (3) complexation between drug and polyelectrolyte is entirely aqueous based, energy minimal, and rapid; (4) complexation process results in high product yield and drug loading; and (5) storage stability for 1 month at 25°C/55% RH was demonstrated for the amorphous nanoplex powder.[68]

(2) In another study with the model drug ciprofloxacin, Kiew et al. worked on preparation and characterization of the drug-polyelectrolyte amorphous nanoplex comparing 2 different polysaccharides, namely dextran sulfate and carrageenan (Fig. 12). The mechanism of preparation is similar to that in case study 1. Five different criteria of the amorphous drug-polyelectrolyte nanoplex were examined, namely: (1) preparation efficiency (drug complexation efficiency, yield, and drug loading); (2) physical characteristics [morphology (i.e., size, shape), colloidal stability, amorphous state stability, and powder flowability after freeze drying]; (3) supersaturation levels in the presence of crystal inhibitors such as HPMC; (4) antimicrobial activity; and (5) cytotoxicity.

The preparation efficiency of amorphous nanoplexes containing dextran sulfate as the polyelectrolyte was higher (due to dextran sulfate having 2 times the charge density of carrageenan); this is reflected in the higher complexation efficiency (85 ± 2%), yield (74 ± 6%), and drug loading (80 ± 3%), compared to those complexes containing carrageenan. The higher charge density of dextran sulfate stimulates the interaction between ciprofloxacin and dextran sulfate. The particle size of dextran sulfate containing nanoplexes (380 ± 30 nm) was more than 6 times greater than carrageenan containing nanoplexes (59 ± 10 nm). The lower size of the carrageenan containing nanoplex is due to (1) lower critical aggregate concentration; (2) faster precipitation time, resulting in fewer complexed drug molecules and hence smaller size; (3) higher hydrophobicity of carrageenan due to the 5 membered cyclic anhydride ring structure, which enhances the tendency of complexes to precipitate out; and (4) the lower charge density of carrageenan, which results in fewer drug molecules complexed to carrageenan compared to dextran sulfate.

The surface potential of the carrageenan containing nanoplexes was lower (−37 ± 1 mV) compared to those containing dextran sulfate (−55 ± 15 mV), indicating the poor colloidal stability of the drug-carrageenan nanoplexes due to the low charge density of carrageenan. The flowability of both nanoplexes was determined to be excellent with Carr's indices <21, suggesting ease of formulating the dry powder into a solid oral dosage form. The maximum achievable supersaturation level in the presence of HPMC in the dissolution medium (pH 7.4 phosphate buffer saline) for dextran sulfate containing nanoplex suspensions was ≈17X the saturation solubility of the drug, which was higher than the carrageenan containing nanoplex suspensions which was ≈11X the saturation solubility of drug for the initial stages of the *in vitro* dissolution testing. Although the particle size of the carrageenan containing

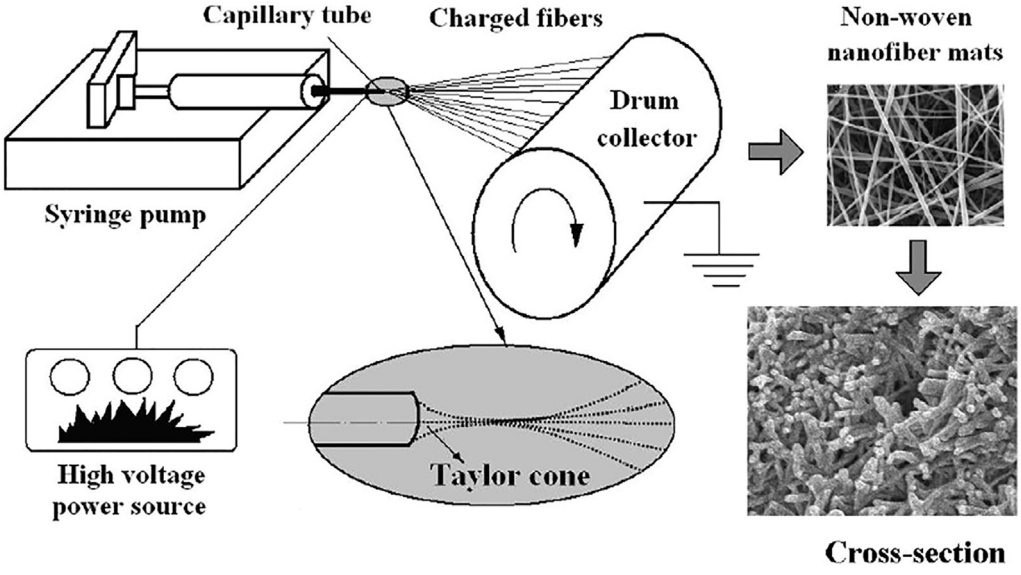

Figure 9. Process of electrospinning. Reproduced with permission from Yu et al.[87]

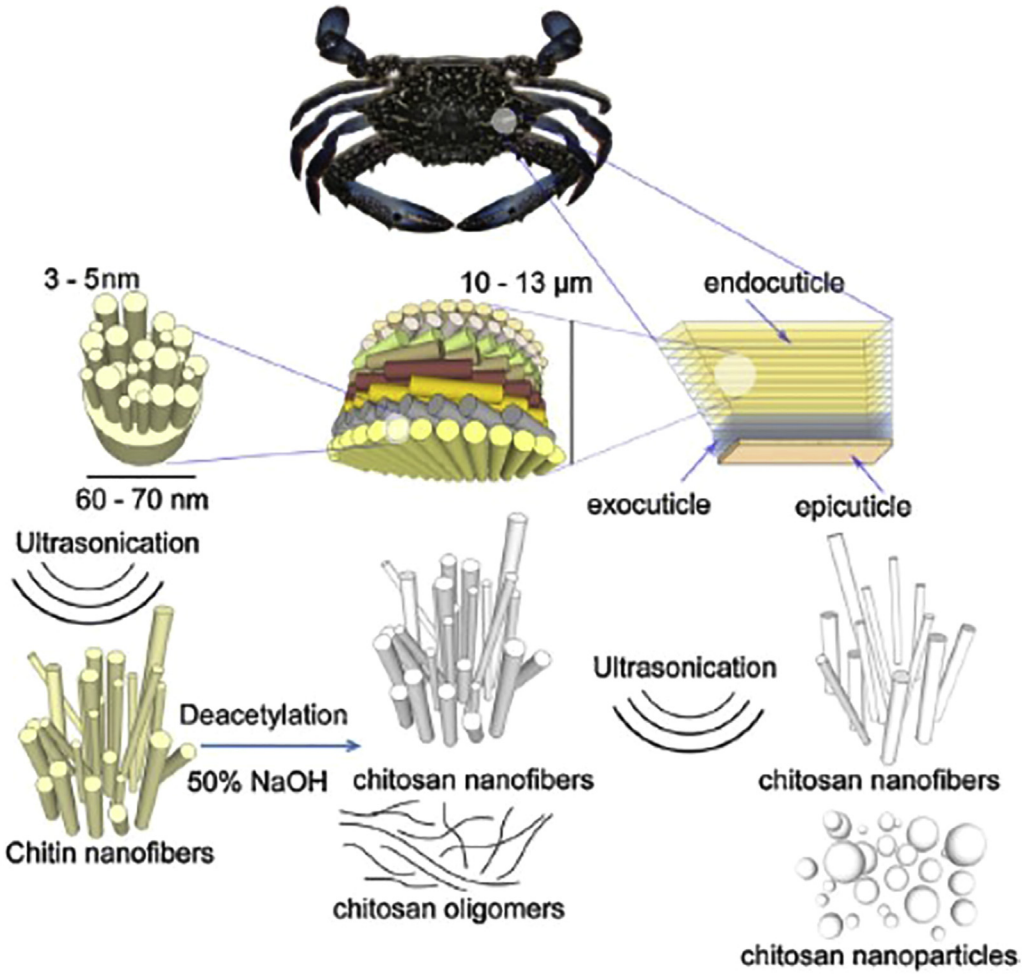

Figure 10. Schematic demonstrating manufacturing of amorphous chitosan nanoparticles. Reproduced with permission from Wijesena et al.[74]

nanoplex suspensions was smaller compared to the dextran containing nanoplex suspensions, during the initial 50 min only 70% of the drug was released from the carrageenan containing nanoplex suspensions compared to 100% drug release from the dextran sulfate containing nanoplex suspensions.

Additionally, the maximum achievable supersaturation level of the dextran containing nanoplex powders was higher (≈8.4X) compared to that of the carrageenan containing nanoplex powders (≈6.5X). However, the supersaturation level for dextran containing nanoplex powder decreased to ≈4X at equilibrium, but the carrageenan containing nanoplex powder maintained the supersaturation level for 210 min after reaching the maximum point. The low solubility of carrageenan in the dissolution medium (pH 7.4 phosphate buffer saline) and the high tendency of carrageenan to form a gel at 37°C were responsible for the slower dissolution rate of drug from the carrageenan containing nanoplexes. Both nanoplexes were determined to be in a stable amorphous solid-state form, were noncytotoxic, and possessed antimicrobial activity.[92]

(3) In another report incorporating polyelectrolytes to prepare amorphous nanoparticles, Yang et al. studied the effect of 2 different amorphization mechanisms on morphology, colloidal stability, drug loading, amorphous solid-state stability (3-month storage) and *in vitro* supersaturation (Fig. 13). Two strategies were employed in the preparation of amorphous nanoparticles, namely: (1) drug-polyelectrolyte complexation to prepare itraconazole-dextran sulfate amorphous nanoplexes and (2) pH shift precipitation, using

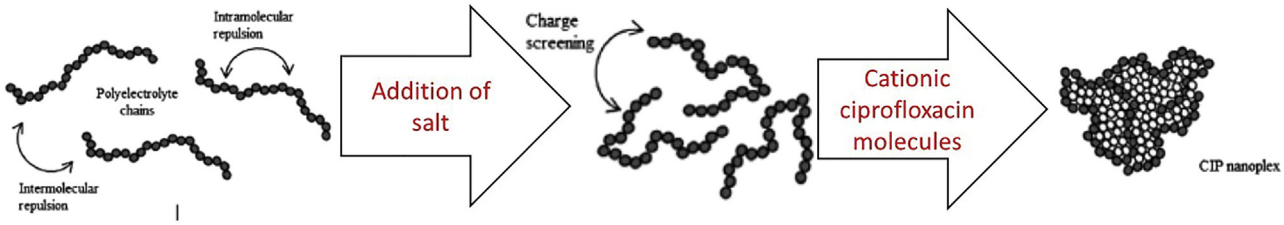

Figure 11. Schematic exemplifying the role of salt in ciprofloxacin nanoplex formation. Reproduced with permission from Cheow and Hadinoto.[68]

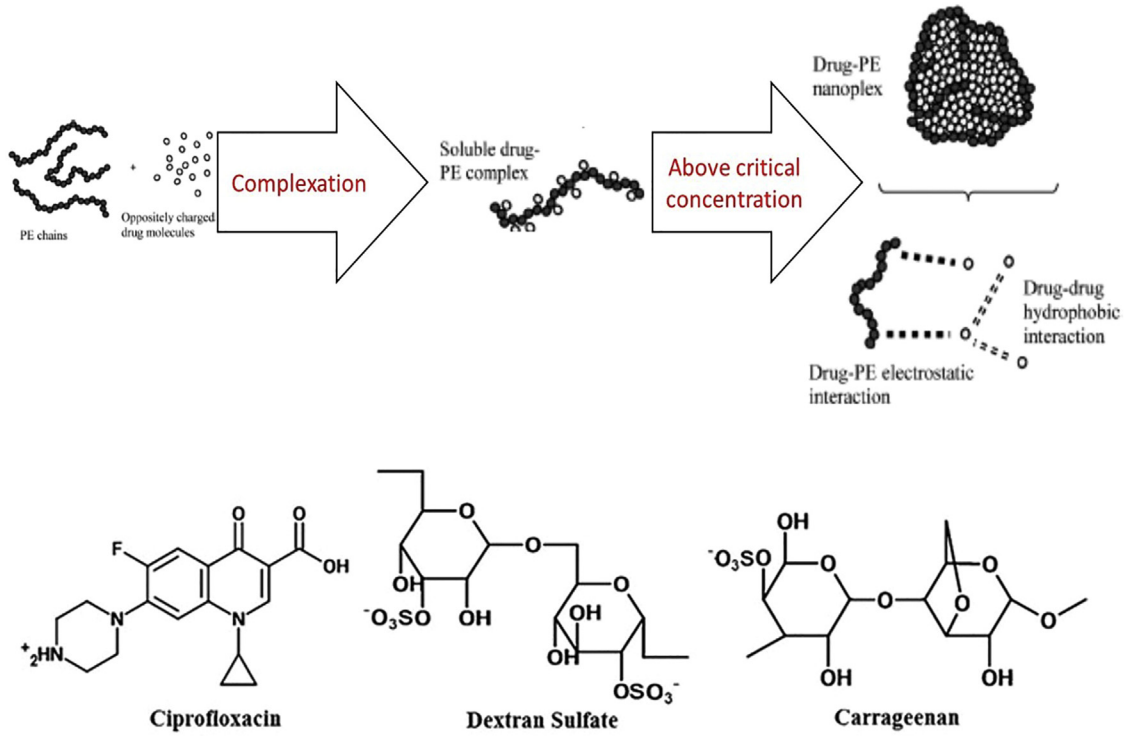

Figure 12. Flow diagram indicating amorphous nanoplex formation comparing 2 polysaccharides. Reproduced with permission from Montes et al.[76]

HPMC as the surface stabilizer to prepare itraconazole nanoparticles.

In the preparation of itraconazole nanoplexes, 2 types of dextran sulfate were screened: low molecular weight (LMW) and high molecular weight (HMW). The average yield of the nanoplexes containing HMW dextran sulfate was ~43% compared to a much lower yield in the case of LMW dextran sulfate (~19%); this difference was due to stronger interactions between HMW dextran sulfate and itraconazole.

The particle morphology using TEM showed that the dry particles prepared via either strategy were spherical in shape with an average size of ~300 nm. The average particle size for amorphous nanoplexes and nanoparticles in the suspension form was ~400 ± 120 and 480 ± 250 nm, respectively. The particle size in suspension form was higher compared to the dry powder due to swelling of the polysaccharide stabilizers (dextran and HPMC) in water. The drug loading of the itraconazole nanoparticles was ~94 ± 7% (wt/wt) compared to ~65 ± 6% (wt/wt) for itraconazole nanoplexes. This difference in loading was due to the smaller amount of HPMC which is adsorbed only on the surface of the itraconazole nanoparticles, compared to the HMW dextran which is present throughout the itraconazole nanoplexes as a result of electrostatic complexation.

The percent yield of the final product was greater in case of the itraconazole nanoplexes (84%) compared to the itraconazole nanoparticles (35%). The low yield of the nanoparticles was due to the nonrecovery of the large particles formed in the pH shift precipitation method as a result of Ostwald ripening. Storage stability of the amorphous systems was evaluated after 3-month storing at 25°C/30% RH. Under PXRD, the itraconazole nanoparticles showed broad diffuse crystalline peaks compared to the raw crystalline drug; however, the itraconazole nanoplexes were determined to be completely stable, displaying a halo pattern indicative of the solid-state amorphous form following 3-month storage stability.

The initial supersaturation level during the first 30 min of *in vitro* dissolution testing of suspensions of the itraconazole nanoparticles was ~10.5X the saturation solubility of drug, compared to the ~8.5X for itraconazole nanoplex suspensions. However, for the powder formulation the supersaturation levels were significantly lower (~4X and ~2.3X) for the itraconazole nanoparticles and nanoplexes, respectively. The lower maximum supersaturation level for the powder formulation may be due to the smaller surface area available for dissolution, because the nanoparticles exist as loose aggregates in the micrometer size; this suggests that all nanoparticles are not in contact with the dissolution medium. The reduced dissolution rate instigates the remaining solid to recrystallize during the dissolution process, reducing the supersaturation level. The presence of recrystallized solids inhibits further supersaturation by Ostwald ripening. Thus, it is necessary to ensure rapid and complete reconstitution of the nanoparticles when they come in contact with the dissolution medium, in order to maintain supersaturation levels for the amorphous nanoparticles for longer periods of time.[71]

Antisolvent Precipitation

Case Studies

(1) Homayouni et al. studied various particle engineering methods for the preparation and characterization of micro/nanoparticles consisting of celecoxib and PVP-K30 at different ratios. The techniques mainly used were spray drying, antisolvent crystallization-freeze drying, antisolvent crystallization-spray drying, and antisolvent crystallization-high pressure homogenization-freeze drying. The physicochemical and pharmaceutical characterization of the different samples were carried out using DSC, PXRD, Fourier transform infrared spectroscopy (FTIR), particle size

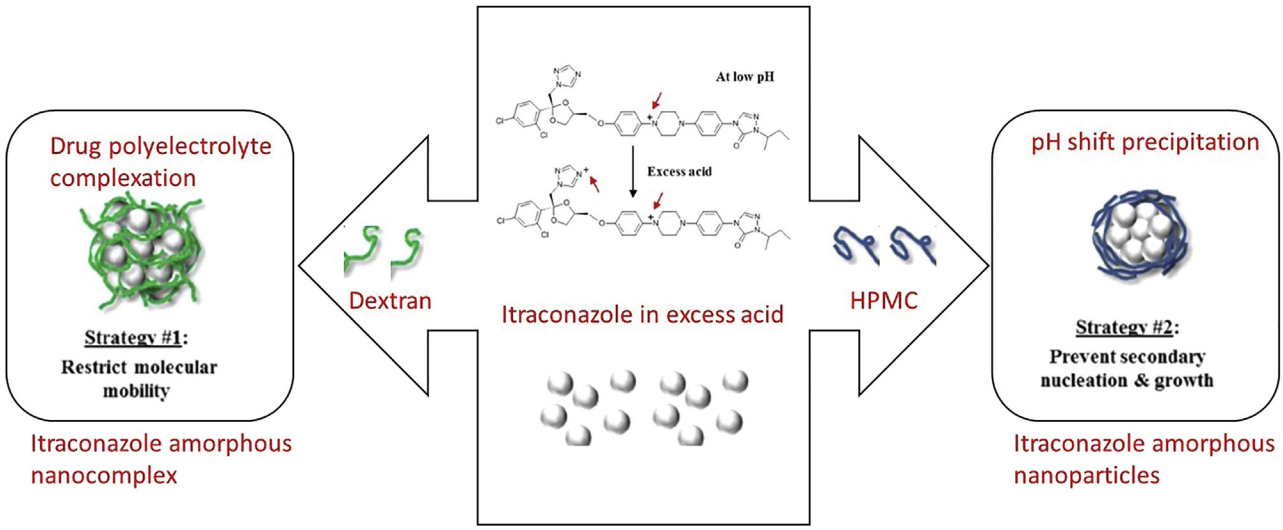

Figure 13. Schematic of 2 amorphization strategies to prepare itraconazole amorphous nanoplexes and nanoparticles. Reproduced with permission from Cheow et al.[71]

measurements, optical and scanning electron microscopy, saturation solubility, and dissolution testing.

The raw crystalline celecoxib revealed a rod-shaped structure under scanning emission microscopy (SEM). Increasing the PVP concentration (from 5% to 50%) during spray drying changed the particle morphology from needle-shaped structures to complete spherical particles with wrinkled surfaces. Additionally, the average size of the microparticles was also reduced. The antisolvent precipitation-freeze drying method [celecoxib:PVP = 95:5] resulted in spherical nanoparticles due to momentary formation of nanoemulsion droplets (quasi-emulsion solvent diffusion), which was followed by the precipitation of the nanocrystals inside the droplets due to counter-diffusion of the solvent-methanol and antisolvent-water out and into the emulsion droplets.

During the antisolvent precipitation-spray drying method, the PVP concentration was increased from 5% to 50% to form stable amorphous nanoparticles. It was observed that at low concentrations of PVP (<25%), the nanoparticles stuck to each other, forming big particles during spray drying; however, at 50% PVP, the number of particles decreased due to the solubilizing effect of PVP. During antisolvent crystallization-high pressure homogenization-freeze drying, nanocrystals were formed as a result of the solvent boiling when passed through the gaps, and the consequent formation of gas bubbles, which implode after leaving the homogenization area and break down the nanocrystals via cavitation. The particle size increased during antisolvent crystallization-high pressure homogenization-freeze drying, and this may be a result of an initial decrease in size due to drug dissolution in methanol followed by recrystallization of the drug during high pressure homogenization. However, the particle size after high pressure homogenization (514 nm) was smaller compared to that obtained following spray drying (3870 nm). Increase in the PVP concentration (5%-25%) increased the particle size from 450 to 1175 nm during high pressure homogenization; this may be attributed to decreased surface charge causing particle aggregation at higher concentrations of PVP.

DSC and PXRD techniques were used to investigate the solid-state forms of the amorphous nanoparticles. The spray-dried celecoxib-PVP displayed a halo pattern under PXRD, confirming the amorphous form. At 5% PVP concentration, using antisolvent crystallization-freeze drying and antisolvent crystallization-spray drying, PXRD profiles showed a halo pattern similar to the raw amorphous celecoxib, confirming the amorphous solid-state form of the product. At 5% PVP concentration, using the antisolvent crystallization-high pressure homogenization-freeze drying technique, the product displayed reduced intensity diffraction peaks, indicating the recrystallization of the celecoxib during high pressure homogenization.

FTIR was used to study the interaction (hydrogen bonding) between the NH2 group of celecoxib and C=O group of PVP. There was a minor shift in the C=O stretching vibration band in celecoxib:PVP samples, which may be attributed to a large number of nonbonded C=O in comparison with the bonded C=O groups.

The dissolution rates were compared for the formulations prepared using different methods. It was observed that the dissolution rate for spray-dried samples containing high PVP concentration (25% or 50%) was higher compared to those prepared with low PVP concentration (5% or 10%), which may be due to the molecular dispersion of drug in the PVP matrix, expediting the formation of glassy solution (confirmed by DSC). In the antisolvent crystallization-freeze drying method, the dissolution rate increased with increase in the PVP concentration, due to the hydrophilic nature of PVP, which enhances the dissolution rate. At lower PVP concentration (5% or 10%), the samples produced using the antisolvent crystallization-freeze drying method showed faster dissolution rates, due to the smaller particle size, resulting in higher surface area. The antisolvent crystallization-high pressure homogenization-freeze drying method had a significant impact on the enhancement of the dissolution rate of celecoxib. Dissolution was independent of the method of preparation at high PVP concentration. While, at low PVP concentration, the dissolution was dependent on the physicochemical properties of the particles (particle size, surface area, etc.) and the method of preparation.[72]

(2) Matteucci et al. reported on the recovery of polymer-stabilized amorphous nanoparticles, from aqueous dispersions using salt flocculation. The antisolvent precipitation method was used to produce flocs of amorphous polymer-stabilized nanoparticles, which were filtered, spray or freeze-dried, and redispersed to obtain the initial particle sizes and to raise the supersaturation levels up to 14 times the crystalline solubility of raw drug.

HPMC and P407 were used as polymers for the preparation of amorphous nanoparticles. Following particle size determination of the nanoparticles, the dispersions were flocculated by addition of 1.5 M Na_2SO_4 solution (volume ratio: 12:5 salt solution/suspension). After filtration, the filter cake was then allowed to dry at room temperature and atmospheric pressure overnight.

In the absence of P407, the average particle size of aqueous dispersions after solvent removal was 1-5 μm. On increasing the concentration of P407, the particle size decreased to a threshold value of 300 nm. The average particle size of the freeze- and spray-dried samples after redispersion containing itraconazole:P407:HPMC (8:1:2) was 700 nm and 5 μm, respectively. DSC was used to determine the solid-state form of the flocculated dried powders. The presence of a glass transition peak for flocculated dried powder verified its amorphous character. The maximum achievable supersaturation level for salt flocculated dried powder was ~14X saturation solubility, in pH 6.8 phosphate buffer with 0.17% SDS. There was rapid crystallization evident from modulated DSC for the control samples [rapidly frozen/lyophilized and spray-dried itraconazole:P407:HPMC (8:1:2)]; thus the lack of recrystallization for the salt flocculated samples is considered to be an advantage for the dissolution process.[64]

(3) Zu et al.[66] worked on preparation and characterization of amorphous amphotericin B nanoparticles for oral administration using liquid antisolvent precipitation, followed by freeze drying (Fig. 14). In a single factor experiment, the effect of 6 factors on the average particle size of amphotericin nanoparticles was investigated, namely, the type and concentration of surfactant (0.15%, 0.25%, 0.35%, and 0.45%); stirring time (1, 5, 15, 30, 60, 90, and 120 min); precipitation temperature (2°C, 12°C, 22°C, and 32°C); stirring intensity (500, 1000, 1500, and 2000 r/min); drug concentration (20, 40, 60, and 80 mg/mL); and volume ratio of antisolvent to solvent (1/1, 7/1 13/1, and 19/1). Dimethyl sulfoxide was used as the solvent and ethanol was used as the antisolvent. Tween 80 and Poloxamer 188 were screened for the preparation of the amorphous nanoparticles.

The average particle size increased from 164.5 to 280.5 nm, when the Tween 80 concentration increased from 0.15% to 0.45%. According to Chi et al.,[65] Tween 80 decreased the average particle size if the drug particle has multiple hydrodynamic domains, which prevent crystal aggregation. However, increasing the concentration of Tween 80 increased the viscosity and slowed down the diffusion process between solvent and antisolvent, leading to slower nucleation rates, and thus the particle size and the Tween 80 concentration had a linear relationship. The optimum concentration of Tween 80 was 0.15%, which may provide the most suitable steric hindrance preventing the nanoparticle growth and agglomeration. For Poloxamer 188, the average particle size reduced from 265 to 211 nm. The particle size decreased gradually with increasing stirring time. Stirring times <30 min caused aggregation and consequent precipitation. Increasing the stirring time above 30 min caused particle size reduction for the larger crystals. Thus the optimum stirring time for preparation of nanoparticles was 30 min. Increasing the precipitation temperature from 22°C to 32°C causes increase in particle size from 164.5 to 311.4 nm, without affecting the solubility. Low temperature accelerates supersaturation levels and nucleation, generating smaller particles. Crystals grew below 4°C, thus for optimum precipitation the temperature was maintained at 12°C.

The particle size reduced from 174.6 to 135.1, when the stirring intensity was increased from 500 to 2000 r/min. With increase in stirring intensity, there was an increase in the micromixing of the multiphases, resulting in a high and homogenous supersaturation in a short period of time. The stirring time was maintained at 2000 r/min. The average particle size increased from 135.1 to 224.3 nm when the amphotericin drug concentration was increased from 20 to 40 mg/mL, due to increase in the viscosity of drug solution, preventing diffusion between solvent and antisolvent and hence increasing the average particle size. The smallest size particles were obtained at a concentration of 20 mg/mL. The average particle size decreased from 317.8 to 135.1 nm as the antisolvent to solvent volume ratio increased from 1:1 to 13:1, due to an increase in supersaturation. The optimum volume ratio was 13:1.

The freshly precipitated and freeze-dried nanoparticles were characterized using SEM, and the particle size of these formulations was determined to be 135.1 and 215.6 nm, respectively, with spherical particle morphology. PXRD characterization supports the fact that the nanoparticles obtained were amorphous in nature. During *in vitro* dissolution testing, the amorphous amphotericin nanoparticles resulted in 2.1X supersaturation level (faster dissolution rates) compared to the raw crystalline amphotericin.[73]

Solvent Evaporation

Case Studies

(1) Hoa et al. prepared ketoprofen amorphous nanoparticles using a solvent evaporation method. The polymer selected was Eudragit E100 (copolymer consisting of 1:2:1 molar ratio of methyl methacrylate, N,N-dimethylaminoethyl methacrylate, and butyl methacrylate monomers). The drug and polymer mixture was dissolved in chloroform under magnetic stirring at room temperature. SDS was added to the above mixture under stirring. Agitation was continued until complete removal of solvent. Lyoprotectants namely glucose and lactose were added to the nanoparticle dispersions, following which freeze drying of the nanoparticle dispersions was carried out.

The particle morphology was investigated using SEM, revealing the spherical and nonaggregating nature of the nanoparticles. The average diameter of the particles was 150 nm based on SEM and DLS data. FTIR spectra analyzed showed that the peak for the carboxylic group in raw crystalline ketoprofen was observed at 1697.03/cm, which was absent in the nanoparticles, confirming that the carboxylic group of the drug interacts with the polymer. The amorphous nature of the nanoparticles was revealed based on the PXRD diffractograms.[65]

(2) Dillen et al. worked on preparation and characterization of PLGA [poly(lactic-co-glycolic acid)]-based ciprofloxacin nanoparticles, prepared by water in oil in water (W/O/W) emulsification solvent evaporation method. Polyvinyl alcohol (PVA) was selected as a stabilizer. A 2^4 full factorial experimental design of experiment (DoE) based on the 4 factors were investigated for their effects on particle size, surface charge, drug loading efficiency, and drug release, namely number of homogenization cycle, addition of boric acid to inner drug containing water phase, ciprofloxacin concentration in the inner water phase, and the oil:water phase ratio.

The nanoparticles were manufactured by a W/O/W emulsification solvent evaporation method followed by high pressure homogenization and freeze drying. The organic solvent used was dichloromethane and the stabilizer solution was PVA. The particle size of the nanoparticles was determined to be 180-275 nm. A

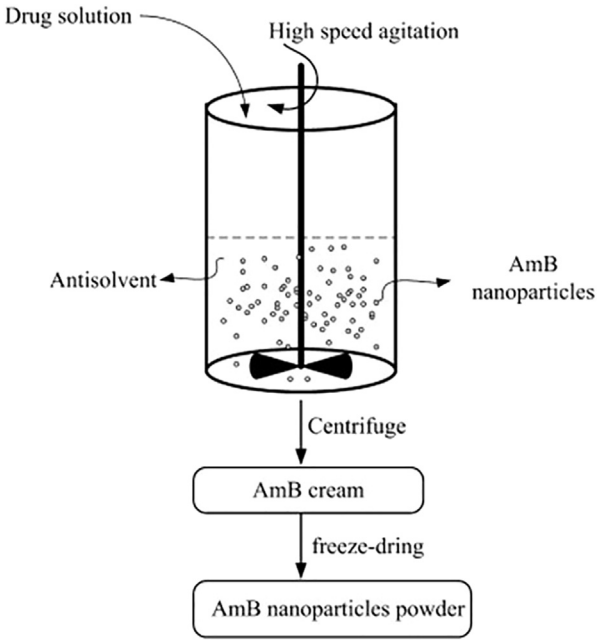

Figure 14. Schematic of experimental process to prepare amorphous amphotericin nanoparticles. Reproduced with permission from Zu et al.[73]

higher number of homogenization cycles resulted in the formation of smaller emulsion droplets leading to the generation of smaller nanoparticles. The range of zeta potential measured in the simulated lachrymal fluid was −3.8 to −10.7 mV. Entrapment efficiencies between 28% and 87% and absolute drug loading levels between 6 and 37.5 μg drug/mg nanoparticles were measured.

Increase in the homogenization intensity resulted in a decrease in the emulsion droplet size and an increase in surface area, with consequent faster removal of dichloromethane and therefore increased encapsulation efficiency. The homogenization process had a contradictory influence on drug release, because increasing the number of homogenization cycles did not only have an effect on the size of the nanoparticles, but also on the drug encapsulation efficiency, which in turn effected the release of ciprofloxacin. Drug release was faster following gamma sterilization of nanoparticles. Addition of boric acid to the inner water phase increased drug release rates, but only after 6.5 h. Drug incorporated in the nanoparticles was amorphous in nature according to the PXRD profiles and DSC thermograms. Microbiological activity tests proved that, although not 100% of the drug incorporated was released from the nanoparticles after 24 h, the nanoparticles and an aqueous solution had comparable activity against *Pseudomonas aeruginosa* and *Staphylococcus aureus*.[60]

Sonoprecipitation

Case Studies

(1) Jog et al.[93] prepared amorphous ABT-102 nanoparticles (ABT-102 is a selective TRPV1 antagonist used in pain management) via sonoprecipitation using 2 different stabilizers (Soluplus and PVP K25). Formulation (e.g., concentration of polymer [Soluplus and PVP K-25], surfactant [sodium lauryl sulfate, SLS] and sugar [trehalose]) and spray drying process parameters (e.g., temperature, aspirator setting, and feed rate) were investigated using a DoE approach. Particle size distribution, moisture content, PXRD, PLM, FTIR, and *in vitro* dissolution were utilized to characterize the spray-dried nanoparticle formulations. The amorphous nanoparticles prepared using Soluplus (particle size 189.3 nm) showed enhanced dissolution rate compared to those prepared using PVP K25 (particle size 148.9 nm) (Fig. 15). Based on the spray drying process and formulation DoE studies, 2 responses (particle size and total yield of spray-dried amorphous ABT-102 nanoparticles) were significant, while the other responses (moisture content and drug loading) were not significant.

Stability studies were performed on the optimized formulations to monitor physical and chemical changes under different temperature and humidity conditions. Following 3-month storage, it was observed that the formulations stored at 4°C were stable in terms of particle size distribution, moisture content, and crystallinity, whereas those stored at 25°C/60% RH and 40°C/75% RH were unstable. The lipophilic poly(vinyl caprolactam) region of Soluplus is able to interact with the drug, while the hydrophilic polyethylene glycol (PEG) region resulted in enhanced wettability of the amorphous nanoparticles, thus increasing the dissolution rate and maintaining higher supersaturation levels (4-fold) compared to PVP K25 (3-fold) (Figs. 15a and 15b). This study shows that amorphous nanoparticles prepared using sonoprecipitation followed by spray drying have an enhanced dissolution rate and may enhance bioavailability compared to macrocrystalline drug.[93]

(2) Kumar et al.[94] formulated nanoamorphous spray-dried powders to enhance oral bioavailability of itraconazole. A critical quality attribute (particle size) was evaluated by investigating critical processing parameters: antisolvent-to-solvent ratio, drug concentration, and stabilizer (surfactant) concentration via DoE studies. Different sugars were screened to prepare a spray-dried stable nanoamorphous formulation. Nanoamorphous powders were characterized via PLM, DSC, PXRD, *in vitro* dissolution testing, and *in vivo* bioavailability studies. The particle size of the nanoformulations was drug concentration dependent (low drug concentration yielded small size precipitates). Stable spray-dried nanoamorphous powders were obtained when disaccharides were used during spray drying, the other HMW sugars and mannitol formulations were unstable and crystallized during spray drying. *In vitro* dissolution testing and *in vivo* studies showed the superior performance (i.e., higher and faster supersaturation solubility) of the nanoamorphous formulations compared to melt-quench amorphous and crystalline itraconazole formulations. The nanoamorphous formulation resulted in a 2.5-fold and 18-fold increase in bioavailability compared to the macroamorphous (melt quench) and macrocrystalline formulations, respectively. The nanoamorphous formulations showed similar bioavailability to the nanocrystalline formulation but with a faster absorption profile (Figs. 16a and 16b).[94]

(3) Dhumal et al.[63] prepared amorphous cefuroxime axetil nanoparticles by sonoprecipitation to enhance oral bioavailability. The cefuroxime nanoparticles prepared by sonoprecipitation were compared with particles prepared by (1) antisolvent precipitation and (2) spray drying. The solvent was acetone and the antisolvent was isopropyl ether. All experiments were carried out at ~5°C, because at low temperature there is rapid precipitation, smaller particle size, and enhanced yield of the final product.

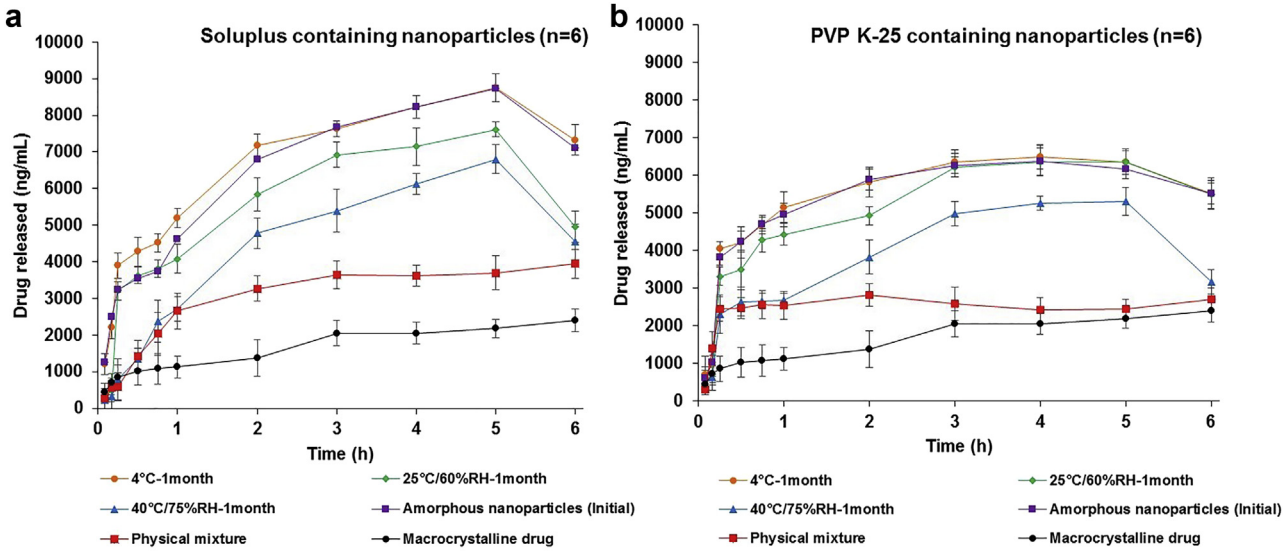

Figure 15. *In vitro* dissolution testing profiles (amount of drug release (ng/mL) vs. time (h)) of the ABT-102 crystalline drug, physical mixture of drug and polymer (PM), and optimized spray-dried nanoparticle formulations prepared using (a) Soluplus and (b) PVP K25. The formulations were filled into hard gelatin capsules and stored under 4°C, 25°C/60% RH and 40°C/75% RH for 1 month.

The average particle size was 130 and 80 nm at 25% and 50% sonication amplitude, respectively (at 5°C for 1 min). The particle morphology was spherical and the product yield was in the range of 95%-98%. When the method of preparation was only antisolvent precipitation, the particle size distribution was broad ranging from 10 to 100 μm, with a product yield of 60%-66%. There was aggregation of fine particles into large particles as observed in the SEM images. The larger particle size during antisolvent precipitation is considered to be due to the use of mechanical stirring. Using this method, the micromixing was poor, leading to an increase in the local precipitation rate causing aggregation and increase in particle size. This is not the case with sonoprecipitation, where the application of ultrasound ensures uniform mixing throughout the vessel resulting in discreet nanoparticle production.

In experiments using spray drying as a method of preparation, the particle size was 10 μm, with a product yield of 55%. In addition, the particle morphology was determined to be spherical and smooth compared to the raw irregular shaped crystalline drug particles. The solid-state form of the nanoparticles was analyzed using DSC and PXRD. The presence of a halo and diffuse pattern in the PXRD diffractograms of nanoparticles produced by all 3 techniques confirmed the amorphous solid-state form. In addition, the absence of a melting endotherm (as observed for crystalline cefuroxime axetil) at 181°C for nanoparticles produced by all 3 methods also indicated the amorphous solid-state form.

During *in vitro* dissolution testing, the unprocessed raw crystalline drug resulted in 45% drug release at the end of 150 min owing to the large crystal size. Spray-dried drug resulted in 70% drug release after 150 min, due to the amorphous nature of the drug. Nanoparticles produced via antisolvent precipitation resulted in 79% drug release after 150 min, due to the amorphous nature of the drug and porous agglomerates, made of fine subunits, increasing the effective surface area for dissolution. Nanoparticles produced by sonoprecipitation resulted in 90% drug release in the first half an hour, followed by complete drug release after 60 min. The reason for the faster dissolution rate was the amorphous nature of the nanoparticles as well as their nanosize and lack of aggregation. The absorption profiles of the sonoprecipitated drug were

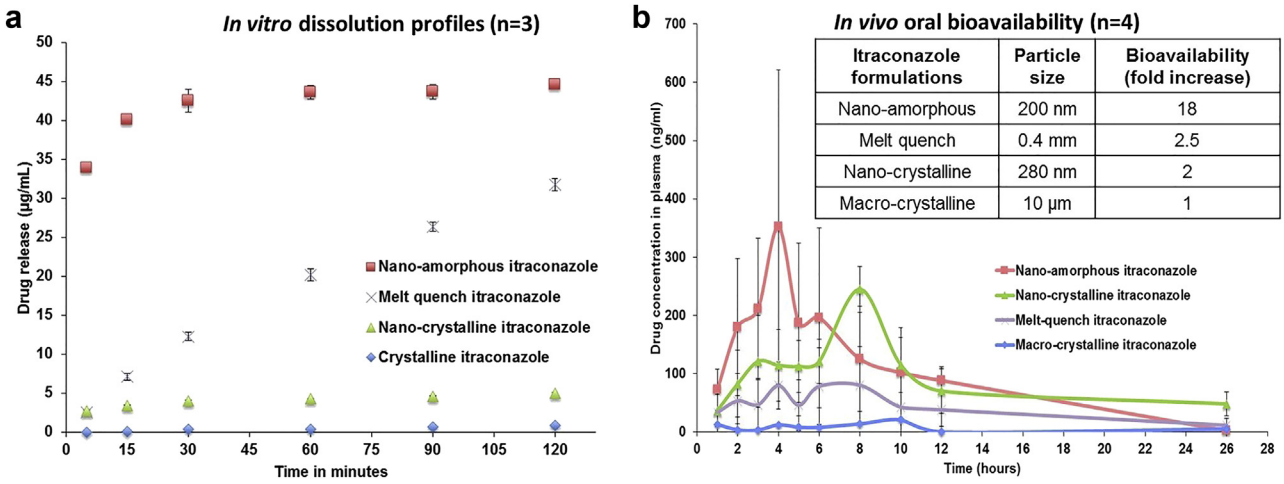

Itraconazole formulations	Particle size	Bioavailability (fold increase)
Nano-amorphous	200 nm	18
Melt quench	0.4 mm	2.5
Nano-crystalline	280 nm	2
Macro-crystalline	10 μm	1

Figure 16. (a) *In vitro* dissolution testing of the spray-dried itraconazole formulations and (b) *in vivo* oral bioavailability study of the spray-dried itraconazole formulations.

Table 4
List of the Methods and Physicochemical Parameters Involved in the Preparation and Characterization of Pharmaceutical Amorphous Nanoparticles

Drug	Excipients	Manufacturing Technique	Particle Size (nm)	Drug Loading (%wt/wt)	Drug Equilibrium Solubility (X) (Aqueous Solubility)	Supersaturation Solubility	Reference
Chitin nanofibrils	Chitosan biocompatible, nontoxic	Direct ultrasonication, top down	<25 (atomic force microscopy) <300 (TEM)	–	–	–	74
Itraconazole	Dextran sulfate polyelectrolyte Hydroxypropyl methylcellulose—surface stabilizer	(1) Drug-polyelectrolyte complexation (2) pH-shift precipitation	400 (Itraconazole nanoplex) 480 (Itraconazole nanoparticles)	(1) 65 (2) 94	1 ng/mL (at neutral pH)	Nanoparticle powder (1) 2.3X (nanoplexes) (2) 4X (nanoparticles)	71
Ciprofloxacin	CGN, DS—anionic polysaccharide HPMC polymer	Electrostatic complexation of charged drug molecules with oppositely charged polysaccharides	59 (CGN) 380 (DS)	60 (CGN) 80 (DS)	0.14 mg/mL	Suspension: In 2 mg/mL HPMC 11X (CGN) 17X (DS) In 4 mg/mL HPMC 6.5X (CGN) 23X (DS) Dry powder: In 2 mg/mL HPMC 6.3X (CGN) 7.6X (DS)	92
Celecoxib	PVP K-30 hydrophilic polymer	(1) Spray drying (2) Antisolvent precipitation followed by freeze drying (3) Antisolvent precipitation followed by spray drying (4) Antisolvent precipitation—HPH-freeze drying	(1) 3761 (2) 344 (3) 2831 (4) 450-1175	–	2.1 μg/mL	–	72
Itraconazole	Lecithin—stabilizing agent	(1) Crystalline nanoparticle—wet ball milling (2) Amorphous nanoparticle—ultra rapid freezing technique	(1) 190 (2) 150	–	1 ng/mL (at neutral pH)	(1) 3X at 30 min, 2X at 6 h, equilibrium after 24 h (2) 26X at 30 min, 7X at 2 h, 5X after 24 h	95
Itraconazole	HPMC—hydrophilic stabilizer	Controlled precipitation into aqueous solution	200-600	33-94	4.4 μg/mL (crystalline itraconazole)	70-80X	96
Ciprofloxacin	Dextran sulfate polyelectrolyte Pluronic F68 stabilizer	Drug-polyelectrolyte complexation	300	10-20 (theoretical)	30 mg/mL	–	97
Itraconazole	HPMC—hydrophilic polymer, P407—nonionic polymer	Antisolvent precipitation and immediate flocculation using sodium sulfate	300	80-94	14 μg/mL (pH 6.8 phosphate buffer + 0.17% wt/wt SDS)	14X	64
Paclitaxel	Chitin—biocompatible, biodegradable, and nontoxic	Ionic cross-linking reaction using TPP	ACN—150 Paclitaxel-loaded ACN—200	55	<0.3 μg/mL (water)	–	98
Cefuroxime axetil	–	Microporous, tube-in-tube microchannel reactor	400	–	Poorly water soluble Freely soluble as sodium salt (145 mg/L)	2X	23

(*continued on next page*)

Table 4 (*continued*)

Drug	Excipients	Manufacturing Technique	Particle Size (nm)	Drug Loading (%wt/wt)	Drug Equilibrium Solubility (X) (Aqueous Solubility)	Supersaturation Solubility	Reference
Celecoxib	HPMC E5—hydrophilic polymer	Antisolvent precipitation under sonication followed by high pressure homogenization	159	80 (theoretical)	3-7 μg/mL	4X	99
Cefuroxime axetil	–	Antisolvent precipitation in a YMCR	30-50 μm (raw drug) 5-50 μm (commercial spray-dried product) 300 (postprecipitation in YMCR)	–	Poorly water soluble Freely soluble as sodium salt (145 mg/L)	1.5X	22
Tibolone	ε-Caprolactone with PSu (fast biodegradable and biocompatible)	O/W solvent evaporation method followed by probe sonication	150-200	2-8	Sparingly soluble in aqueous buffer	–	100
Ciprofloxacin	PLGA biodegradable	W/O/W emulsification solvent evaporation method	180-275	28-87	35 mg/mL in water	–	60
β-carotene	EPL biodegradable, biocompatible, low cytotoxicity, nonmutagenic, PEI cationic polymer exhibiting high charge density, chitosan—biocompatible, low toxicity, and low immunogenicity	Turbulent mixing and flash nanoprecipitation	<100	80-90	Water insoluble	Not investigated	66
Amphotericin B	Tween 80, Poloxamer 188—surfactant	Liquid antisolvent precipitation followed by freeze drying	215.6	–	Insoluble in water at pH 6-7, but soluble in water at pH 2 or 11	13X	73
Ezetimibe	Tween 80—surfactant as a stabilizer	Solvent-antisolvent precipitation method	700	80-90	Insoluble in water	3X	101
Cefuroxime axetil	–	Controlled nanoprecipitation	300	–	Poorly water soluble Freely soluble as sodium salt (145 mg/L)	Spray-dried drug (commercial product—63% release in 150 min) was compared against nanoparticles prepared by controlled nanoprecipitation (90% release in 150 min)	21
Cefuroxime axetil	–	Sonoprecipitation	130 (25% sonication amplitude) 80 (50% sonication amplitude)	–	Poorly water soluble Freely soluble as sodium salt (145 mg/L)	Release in 150 min; unprocessed drug 45%; spray-dried drug 70%; mechanical stirred drug 79%; sonoprecipitation 100%	63
Cyclosporine A	L-α-phosphatidylcholine, PVP 40000, PVP K-15, Pluronic F127 stabilizers Brij 97, Myrj 52, Tween 80, PEG 8000, PEG 18500—surfactants	Evaporative precipitation into aqueous solution	100-1200	–	Slightly soluble in water (0.00581 mg/mL)	–	19
Ketoprofen	Eudragit E100	Emulsion solvent evaporation method	50-200	–	Poor solubility in water (0.5 μg/mL)	–	65
Atorvastatin calcium	–	SAS process	152-863	–	Slightly soluble in water (143 μg/mL)	3.2-3.3X (maintained for 3 h)	102
Silymarin, β-carotene, and	–	Nanoporous membrane extrusion	75 ± 27 (silymarin), 102 ± 23 (β-carotene), and 130 ± 30	–	Sparingly solube in water: 0.25 mg/mL for silymarin,		69

butylated hydroxytoluene			(butylated hydroxytoluene)		0.6 mg/mL for β-carotene, and 1.1 μg/mL for butylated hydroxytoluene	3.5X (silymarin) 1.5X (butylated hydroxytoluene)	
Celecoxib	Soluplus—stabilizer and stabilizing agent	Antisolvent precipitation and high pressure homogenization	200-1250	–	Poor aqueous solubility: 1-3 μg/mL	~2X	72
Ciprofloxacin	Dextran sulfate—biocompatible and biodegradable natural polyanion, oppositely charged polyelectrolye	Self-assembly drug—polyelectrolyte complexation process	200-300	80	Sparingly soluble in water: 0.12 mg/mL	2X	68
Glibenclamide	HPMC—hydrophilic stabilizer	Antisolvent precipitation using the high gravity technique	220-270	–	Low aqueous solubility (~38 μmol/L at 37°C)	10X	103
Isradipine	PEO-N 60K, HPMC 6 cps, HPMC 4000 cps—stabilizers	Sonoprecipitation	50	–	Insoluble in water	–	104
Itraconazole	Dowfax 2A1 anionic surfactant	Antisolvent-solvent precipitation	200	–	1 ng/mL (at neutral pH)	2.5X	94
Cyclosporin A	Kolliphor® TPGS	Wet bead milling	350	104	Slightly soluble in water (0.00581 mg/mL)	6.3X	105
Levofloxacin	Stearic acid (lipid), Tween 80 (surfactant), sodium deoxycholate (cosurfactant)	Probe sonication followed by solvent evaporation	237.82	78.71	Slightly soluble in water (1.44 mg/mL)	–	106
Itraconazole	Glutaric acid, malic acid, tartaric acid, citric acid, Kollidon® CL (disintegrant)	Supersolubilization of drug in nonsalt-forming weak acids	450-1000 (pH 5.5)	–	4 ng/mL (25°C)	Itraconazole-glutaric acid solid dispersions 2% and 14% drug load: 80X 20% drug load: 60X	107
Curcumin	Chitosan (polysaccharide), disuccinimidyl tartrate (cross-linking agent)	Ultrasonication of nanosuspension complex	306 ± 14	78.5 ± 1.7	<0.1 mg/mL	–	108
Famotidine	Mesoporous silica nanoparticles, ethylene cellulose, HPMC K15M	Concentrated solvent evaporation	–	52.8		–	109
Vanillin	Polylactic acid (biodegradable)	Single emulsion-solvent evaporation	240 ± 21	41 ± 4	10 mg/mL	–	110
Metformin	Glycerol monostearate, hydrogenated lecithin, polyvinyl alcohol	Double emulsification-solvent evaporation employing cold homogenization	195.01 ± 6.03	29.30 ± 2.29	300 mg/mL (pH range 1.2-6.8)	–	111
734THIF (2° metabolite of daidzein)	EE, PVA	Nanoprecipitation method	734THIF:EE:PVA = 1:8:8 (57.53 ± 2.49), 1:4:4 (106.73 ± 3.21), 1:2:2 (167.2 ± 24.87)	734THIF:EE:PVA = 1:8:8 (83.45 ± 2.33), 1:4:4 (57.23 ± 7.37), 1:2:2 (51.57 ± 1.73)	40 μg/mL (pH 7.4)	4.71X (in stratum corneum) >5.05X (through epidermal and dermal layers)	112
Lercanidipine hydrochloride	PEG 400, hypromellose E15, polyvinyl alcohol, sodium alginate, methyl cellulose, TPGS 1000	Evaporative antisolvent precipitation	Using PEG 400 (314-1263), using TPGS 1000 (277-606)	74.33-96.83	<5 μg/mL (pH > 5)	6.5X	113
Ibuprofen	Witepsol E85 and Miglyol 812, ratio 7:3 (mixture of solid-liquid lipids), Lutrol F68 (surfactant)	Hot high pressure homogenization method	106 ± 1.7	98.51 ± 4.1	21 mg/L (25°C)	2.59X	114
Itraconazole	Pectin (polymeric emulsifier), caprylic/capric triglyceride	Mechanical homogenization followed by freeze drying	500-600	80-87	~1 ng/mL (neutral pH), ~4-6 μg/mL (pH 1)	10X	115
Dihydroartemisinin	Stearic and palmitic acid (solid lipid matrix), PVA,	Single emulsion-solvent evaporation followed by spray drying	240.7	62.3	134.8 μg/mL (25°C)	–	116

(*continued on next page*)

Table 4 (*continued*)

Drug	Excipients	Manufacturing Technique	Particle Size (nm)	Drug Loading (%wt/wt)	Drug Equilibrium Solubility (X) (Aqueous Solubility)	Supersaturation Solubility	Reference
	Tween 20, Tween 80, and DTAB (surfactants)						
Docetaxel	TPGS (vitamin E emulsifier), PLA (biodegradable polymer)	Modified nanoprecipitation method	209.4 ± 5.1	88.47 ± 1.95	0.0127 mg/mL	–	117
Ciprofloxacin	Dextran sulfate, Pluronic F68, α-lactose monohydrate and mannitol	Drug-polyelectrolyte complexation followed by spray drying	300 ± 40	70-80	0.311 mg/mL (25°C)	–	97
Ciprofloxacin	Starch, Tween 80, and Span 80	Emulsion cross-linking technology involving high pressure homogenization and spray/vacuum freeze drying	–	40 (coating method) 7 (adsorption method)	0.311 mg/mL (25°C)	–	118
Cisplatin	PLGA (biodegradable polymer)	Single step electrohydrodynamic atomization	630 ± 95 (0.1%wt/wt drug) 550 ± 80 (0.2%wt/wt drug)	75 (0.1% wt/wt drug) 72 (0.2% wt/wt drug)	2.5 mg/mL (25°C)	–	119
Hydroquinone	Precirol® ATO 5 (glycerol palmitostearate solid lipid), Poloxamer® 407, Span® 20, and Carbopol® 934 (emulsifiers)	Hot emulsification under homogenization	86	89.5	72 mg/mL (25°C)	–	120
Curcumin	PLGA (biodegradable polymer), PVA	Modified single emulsion-solvent evaporation technique	181.5-206.9	58.1-83.2	~1 μM (neutral aqueous solutions)	–	121
ABT-102 (TRPV1 antagonist, analgesic)	Soluplus/SLS, PVPK25/SLS, trehalose	Sonoprecipitation followed by spray drying	189.3 (Soluplus/SLS) 148.9 (PVPK25/SLS)	13 (Soluplus) 11 (PVP K25)	~0.05 μg/mL	4X (Soluplus/SLS) 3X (PVP K25/SLS)	93
Sodium cromoglycate	Chitosan (biocompatible polymer), mannitol	Ionic gelation method followed by freeze drying	200.4 ± 4.06	62.68 ± 2.4	100 mg/mL (25°C)	–	122
Sorafenib	Chitosan, Pluronic F68, PEG, and heparin	Phase transition method, probe sonication followed by freeze drying	185 ± 3.56	78.25 ± 4.65	0.00171 mg/mL	–	123
Timolol maleate	Ethyl cellulose, Pluronic P123, PVA	Double emulsification technique, probe sonication followed by rotary evaporation	1:1—261 1:2—397 1:3—340 (drug:ethyl cellulose, wt/wt)	–	2.74 mg/mL	–	124
Paclitaxel	Amorphous chitin, TPP	Ionic cross-linking	200 ± 50	55	0.3 μg/mL	–	98
Piperolactam A	2-Hydroxypropyl-β-cyclodextrin	Complexation with cyclodextrin, followed by rotary evaporation and lyophilization	180.4 ± 16.42	–	Poor aqueous solubility	–	125
Ibuprofen, calcium phosphate	Poloxamer P407	Spray drying	141.8 ± 14.12 (ACP NPs), 200 ± 0.01 (IBU-ACP NPs)	92	21 mg/L (25°C)	3X	126
Curcumin, Docetaxel, 5-flurouracil	Amorphous chitin, TPP	Ionic cross-linking followed by lyophilization	275 ± 50 (AC-NPs), 250 ± 50 (CUR-AC-NPs), 200 ± 50 (DOC-AC-NPs), and 160 ± 50 nm (5-FU-AC-NPs)	98 ± 1 (CUR-AC-NPs), 77 ± 2 (DOC-AC-NPs) and 47 ± 12 nm (5-FU-AC-NPs)	Curcumin ~1 μM (neutral aqueous solutions); docetaxel 0.0127 mg/mL; 5-flurouracil 12.2 mg/mL	–	127
Ketoprofen	SBA-15 (mesoporous silica), Pluronic P123	Immersion-rotavapor method	5.45 (pore diameter)	54.40 ± 0.1	51 mg/L (22°C)	2.5X	128
Chlorambucil	Egg yolk L-α-lecithin, bovine serum albumin, mannitol	Modified desolvation-ultrasonication technique, followed by lyophilization	144.33 ± 2.17	86.35 ± 2.33	12.4 mg/mL (25°C)	7X	129
Anacetrapib	TPGS 1000 (surfactant), Copovidone (Kollidon VA 64)	Hot melt extrusion	50-200	–	<1 mg/mL	–	130
	PVA, hydroxyapatite		110.10	44.53	120 mg/L (25°C)	–	131

Methyl prednisolone acetate		Chemical precipitation followed by ball milling				
Econazole nitrate	PVP K30, MβCD, HPβCD, Poloxamer P407, PEO, Tween 80, Cremophor EL	Nano spray drying technique	121-1565	42.72-52.11	<0.5 μg/mL	2.66X [132]
Naringen	Egg-phosphatidylcholine, mannitol, glycerol monostearate	Modified emulsification and low-temperature solidification method, lyophilization	98	79.11	~46 ± 6 μg/mL	2.53X [133]
Fenofibrate, griseofulvin, naproxen, phenylbutazone, azodicarbonamide	HPMC E15, SDS, glycerin	Wet stirred media milling, followed by casting and film forming	130-370	–	At 25°C, μg/mL: fenofibrate 0.8, griseofulvin 8.6, naproxen 15.9, phenylbutazone 34, azodicarbonamide 35	– [134]
Pravastatin	Chitosan, STPP	Ion gelation method	129.8 ± 10.5 to 270.4 ± 23.3	49.05-72.04	0.242 mg/mL	– [135]
Ciprofloxacin	Starch	Acetylation and nanoprecipitation	350	20-90	0.311 mg/mL (25°C)	– [136]
Curcumin	DMC, TMC, STPP	Emulsification	DMC/TPP 316.4, TMC/TPP 98.8	DMC/TPP 96.5 ± 0.1, TMC/TPP 99.9 ± 0.2	Curcumin ~1 μM (neutral aqueous solutions)	– [137]
Naringen	Sulfobutylether-β-CD, chitosan	Ion gelation technique	446.4 ± 112.8	67.10 ± 0.26	~46 ± 6 μg/mL	4.6X [138]
Amoxicillin	Chitosan-N-Arginin, γ-PGA-g-Arginin	Electrostatic complexation	<300	38.2 ± 2.4	4 mg/mL	– [139]
Cefixime	0.1 M NaOH, 1 M HCl	High-gravity reactive precipitation followed by spray drying	45	–	55.11 mg/L	11X [140]
Asiatic acid tromethamine	Glycerin monostearate (solid lipid), Poloxamer 188 (surfactant)	Modified solvent injection method	237	64.4	0.03 mg/mL	2.5X [141]
Fenofibrate	–	Supersonic spray drying with a microfluidic nebulator	14	–	0.25 mg/mL (25°C)	– [54]
Rapamycin	Compritol (glyceryl behenate), Tween 80	(1) Modified cold high pressure homogenization (2) Ultrasound-assisted emulsion	(1) 594-751 (2) 93-267	(1)43.8-77 (2)37.5-43.8	2.6 μg/mL	– [142]
Celecoxib	Lipoid E80 phospholipid, egg lecithin, trehalose dihydrate	(1) Spray drying (2) Freeze drying	(1)<1 μm (2)>1 μm	–	3.3 mg/L	(1) 17X (FaSSIF), 18X (PBS) (2) 4X (FaSSIF), 3X (PBS) [143]
Ixabepilone	PEG 2000, Poly(propylene succinate)	Double emulsification and solvent evaporation followed by lyophilization	195	38.8	0.00352 mg/mL	3.5X [144]
Curcumin	(1) Starch, (2) cellulose, (3) cellulose/hemicellulose, TFA	Acid precipitation followed by freeze drying	(1) 10.1 ± 2.5 (2) 25 ± 3.7 (3) 11.7 ± 2.1 (hydrodynamic radius)	(1)23 (2)13 (3)31	Curcumin ~1 μM (neutral aqueous solutions)	– [145]
Diclofenac sodium	Starch, STPP, Tween 80	Modified nanoprecipitation	21.04	95.01	50 mg/mL	– [146]
Xanthoceraside	Silica spheres, hydrofluoric acid	Green ultrasonic method	200	–	Poor aqueous solubility	4.5X [147]
Felodipine	PVP K30-core, HPMC K4M-coating	Ultrasonication followed by rotary evaporation	<150	–	19.17 mg/L at 25°C	6.6X [148]
Cefuroxime axetil	–	RESS	158-513	–	0.107 mg/mL	2X [149]
Phenytoin	–	RESS-solid cosolvent (menthol)	120 (96 bar) 75 (196 bar)	–	32 mg/L (22°C)	400X (compared to RESS) [150]
Griseofulvin	–	RESS-solid cosolvent (menthol)	50-250	–	1 μmol/mol (37°C)	28X (compared to RESS) [151]

(*continued on next page*)

Table 4 (*continued*)

Drug	Excipients	Manufacturing Technique	Particle Size (nm)	Drug Loading (%wt/wt)	Drug Equilibrium Solubility (X) (Aqueous Solubility)	Supersaturation Solubility	Reference
Naproxen	–	Pulsed RESS	200	–	15.9 mg/L	–	152
Cyclosporine	–	RESS	<1000	–	0.006 mg/mL	–	153
Ezetimibe	Hydroxypropyl cellulose, PVP K30	SAS	150-230	95-97	2.26 μg/mL	9.9X	154
Atorvastatin calcium trihydrate (Form I)	–	SAS	100-500 (SEM) 100-900 (DLS)	–	<1 mg/mL	3.3X	102
Minocycline hydrochloride	–	SAS	100-1000	–	52 mg/mL	–	155
Nalmefene hydrochloride	–	SAS	200-300	–	130 mg/mL	–	156
Naproxen	–	SAS	80-1300	–	15.9 mg/L	–	157
Amoxicillin	–	SAS	350-430 (100-250 bar)	–	3.43 mg/mL	–	158
Amoxicillin	–	SAS	250-1200	–	3.43 mg/mL	–	159
Amoxicillin trihydrate	–	SAS	300-1200	–	3.43 mg/mL	–	160
Ampicillin	–	SAS	100-300	–	10.1 mg/mL	–	161
Hydrocortisone	–	SAS-EM	180	–	0.28 mg/mL	–	162
Rifampicin	–	SAS	400-1000 (120 bar)	–	2.5 mg/mL	–	163
10-Hydroxy camptothecin	–	SAS	180 ± 20.3	–	–	11X	164
Atorvastatin hemicalcium trihydrate	–	SAS	68-95	–	Insoluble	4X	165
Lysozyme, myoglobin	–	GAS	50-2000	–	10, 20 mg/mL	–	166,167
Lysozyme	–	GAS	200-300	–	10 mg/mL	–	168
Cefixime	–	GAS	57	–	55.11 mg/L	22.8X	169
Ketoprofen	TEOS, Pluronic P123	Mesoporous silica (SBA-15)	5.45	54.4	51 mg/L	2.5X	128
Rifampicin	TEOS, CTAB	Mesoporous silica	218 ± 46	52	2.5 mg/mL	–	170
Methotrexate	TMAOH, CTAB	Mesoporous silica (MCM-41)	2.95	48	1 mg/mL (19°C)	7X	171
Oxcarbazepine	TEOS, Pluronic F127	Mesoporous silica (SBA-16)	120	17.38	308 mg/L	–	172
Telmisartan	TEOS, CTAB, MMA, APTES	Mesoporous silica	90	60	Insoluble	–	173
Mitoxantrone	TEOS, MPTMS, APTES, CTAB	Mesoporous silica	86-138	18	0.734 mg/mL	–	174
Acetaminophen	PVP K25, ethyl cellulose	Electrospinning Coaxial electrospinning	570 ± 140 910 ± 220	11.11 20.83	14 mg/mL at 25°C	–	175
Acetazolamide	Lutrol F127 (Lu), PCL	Electrospinning	710 (PCL) 550 (Lu:PCL 50:50)	1.24 1.16	0.98 mg/mL	–	176
Timolol maleate	Lutrol F127 (Lu), PCL	Electrospinning	560 (Lu:PCL 50:50)	0.88	2.74 mg/mL	–	176
Itraconazole	HPMC	Electrostatic spinning and milling	300-500	12	~1 ng/mL (pH 7)	–	89
Naproxen Indomethacin Ibuprofen Sulindac	Cellulose acetate	Electrospinning	263-297	84-93	15.9 mg/L 0.937 mg/L 49.0 mg/L Insoluble (pH < 4), 3 mg/mL (pH ≥ 6)	Naproxen > Ibuprofen > Indomethacin > Sulindac	177
Itraconazole	Polyurethane	Electrostatic spinning	300-700	40	~1 ng/mL (pH 7)	–	178
Ketanserin			500-2000	10	5 μg/mL (pH 7)		
Sodium salicylate Diclofenac sodium Naproxen Indomethacin	Polyvinyl alcohol	Electrospinning	107.8 ± 34.8 104.7 ± 26.1 127.4 ± 32.6 165.7 ± 39.0	20	250 mg/mL 50 mg/mL 15.9 mg/L 0.937 mg/L	Sodium salicylate > Naproxen > Diclofenac sodium > Indomethacin	179
Chitosan	PVP	Elevated temperature electrospinning	77 ± 11	–	Insoluble	–	180
Paclitaxel	PLGA (L:G-50:50)	Electrospinning	770 ± 13	9.2 ± 0.03	<0.1 g/mL	–	181
Ketoprofen	PVP K30	Electrospinning	400-600	10	51 mg/L	60X	182
Caffeine Riboflavin	Polyvinyl alcohol	Electrospinning	260-370	–	16 mg/mL 0.1 mg/mL	–	183
Paracetamol Caffeine	PVP K60	Electrospinning	400-750	88-99	14 mg/mL 21.6	–	184

Itraconazole	Kollidon VA64	Electrospinning (single needle, scaled-up high speed)	500-2000	40	~1 ng/mL (pH 7)	9X	185
Cefoxitin sodium	PLGA/PLA/PEG-b-PLA	Electrospinning	260 ± 90	5	0.195 mg/mL	–	186
Ferulic acid	PVP, SDS, sucralose	Electrospinning	254 ± 32	30	0.54 mg/mL	48X	187
Helicid	PVP K60, mannitol	Electrospinning	400-600	5	8.9 mg/mL (20°C)	26X	188
Acetaminophen	Kollidon K90	Electrospinning	300-800	10.321 ± 0.008 mg	14 mg/mL	3X	189
Borneol	PVP K60	Electrospinning	400-800	9%-33%	1.2 mg/mL	–	190
Spironolactone	Soluplus	Electrospinning	300-900	10-20	28 μg/mL	2X	191
Spironolactone	Hydroxypropyl-β-cyclodextrin, PVP K90	Electrospinning	100-1000	20-40	28 μg/mL	4X	192
Curcumin	Polyvinyl alcohol, β-cyclodextrin	Electrospinning	250-350	5-20	<0.1 mg/mL	2X	193
Carvedilol	Eudragit® E	Solvent-free melt electrospinning	700	20	0.583 mg/L	8X	194
Ibuprofen	PVP K30	Electrospinning	800-2000 600-1500	7.5 15	49.0 mg/L	20X	195
Ibuprofen	PVP K30	Electrospinning	40-200	15	49.0 mg/L	–	196
Diclofenac sodium	Eudragit® L100-55	Electrospinning	350-450	9-33	50 mg/mL	–	197
Aceclofenac sodium	Zein (plant protein)	Electrospinning (single nozzle)	50-200	35.98 ± 2.3	–	–	198
Pantoprazole sesquihydrate sodium	Eudragit® S100	Electrospinning (single nozzle)	50-200	33.16 ± 1.4	0.495 mg/mL	–	

734THF, 7,3′,4′-trihydroxyisoflavone; AC, amorphous chitin; ACN, amorphous chitin nanoparticles; ACP, amorphous calcium phosphate; APTES, 3-aminopropyltriethoxysilane; CGN, K-carrageenan; cps, centipoise; CTAB, cetrimonium bromide; CUR-AC, curcumin amorphous chitin; DMC, dimethyl chitosan; DOC-AC, docetaxel amorphous chitin; DS, dextran sulfate; DTAB, dodecyl trimethylammonium bromide; EE, Eudragit E100; FU-AC, 5-flurouracil amorphous chitin; HPH, high pressure homogenization; HPβCD, hydroxypropyl β-cyclodextrin; IBU-ACP, ibuprofen amorphous calcium phosphate; MβCD, methyl-β-cyclodextrin; MCM-41, mobile composition of matter no. 41; MMA, methyl methacrylate; MPTMS, (3-mercaptopropyl)trimethoxysilane; NP, nanoparticle; O/W, oil in water; PCL, polyε-caprolactone; PEO-N, polyethylene oxide N-60K; PGA, poly(γ-glutamic acid); PLA, polylactic acid; PSu, propylene succinate; SAS-EM, supercritical antisolvent enhanced mass transfer; SBA, Santa Barbara amorphous type material; STPP, sodium tripolyphosphate; TFA, trifluoroacetic acid; TMAOH, tetramethylammonium hydroxide; TMC, trimethyl chitosan; TPGS, tocopheryl polyethylene glycol succinate; TPP, pentasodium tripolyphosphate; YMCR, Y-junction microchannel reactor.

one-half fold greater than the spray-dried drug and 2-fold greater than the crystalline drug.[63]

Advanced Methods

Flash Nanoprecipitation
Case Study

(1) Zhu et al.[66] reported on stabilizing drug nanoparticles via polyelectrolytes using a flash nanoprecipitation technique. Three different types of multiamine containing polyelectrolytes [ε-polylysine (EPL), poly(ethylene imine) (PEI), and chitosan] were explored for electrosteric stabilization of the β-carotene nanoparticles. Tetrahydrofuran (THF) was used as a water miscible solvent. Upon providing higher mixing velocities, a better homogeneity of supersaturation was achieved, resulting in a uniform nucleation rate and hence smaller particles with narrow size distribution. During mixing, particle agglomeration was prevented by the kinetic energy of the particles, which is increased due to the higher density of energy dissipation upon faster mixing.

β-Carotene nanoparticles in water were determined to be unstable in the absence of polyelectrolytes. The positively charged water-soluble polyelectrolyte, EPL, was expected to adsorb on the nanoparticle surfaces, acting as electrostatic and steric stabilizers preventing particle agglomeration. However, due to the low charge density of EPL, its absorption on the nanoparticle surfaces was determined to be low. The average particle size was <200 nm for the EPL-β-carotene nanoparticles; however, the particles sedimented in the presence of saline.

The second polyelectrolyte selected for stabilizing the β-carotene nanoparticles was PEI, a linear polymer with a higher density of amino groups and higher molecular weight compared to EPL. Linear PEI lead to particle aggregation. Branched PEI produced spherical particles; however, significant aggregation was associated with LMW branched PEI, followed by sedimentation upon addition of saline. Nanoparticle stability was investigated at various pH conditions, pH 4, 7, and 9. The degree of protonation of the PEI chains at pH 9, 7, and 4 are 10%, 30%, and 65%, respectively. At pH 7 and 4, the nanoparticles were stable over the 5-week study period (as a result of steric repulsion) and had a particle size <200 nm. At pH 9, in the presence of saline, the particle size increased rapidly, indicating that the suspension was unstable and the β-carotene nanoparticles lacked both electrostatic and steric stabilization; this may be associated with the low protonation degree (10%) of PEI chains at pH 9.

The third polyelectrolyte selected for stabilization of the β-carotene nanoparticles was chitosan. Chitosan is water insoluble under neutral and basic conditions, and therefore the experiments were performed at pH 4 (acidic solution). Two chitosan molecular weights, 50 and 250 kg/mole, were investigated. SEM images showed that the nanoparticles were better dispersed with 250 K chitosan compared to 50 K chitosan, even though the particle size (60 nm) was same for both in the absence of saline. Higher molecular weight chitosan provided better steric stabilization. In the presence of saline, the particle size was <200 nm for at least 1 week, stabilizing the β-carotene nanoparticles, with a drug loading of 90%.

The amorphous nature of the solid state was determined using PXRD. All β-carotene nanoparticles produced using flash nanoprecipitation were determined to have halo patterns, characteristic of the amorphous form. THF diffuses instantaneously into water, and therefore there is insufficient time for the large β-carotene molecules to align and pack tightly.[66]

Nanoporous Membrane Extrusion
Case Study

(1) Guo et al.[69] investigated a novel method to prepare amorphous nanoparticles of hydrophobic drugs using NME. Three poorly soluble model drugs, namely silymarin, β-carotene, and butylated hydroxyltoluene were investigated. Particle morphology, crystallinity, and dissolution profiles were investigated. Anodized aluminum oxide (20 and 200 nm on the entrance and exit sides) was selected as a nanoporous membrane, which was sandwiched between 2 half U-tubes. The feed solution was the model hydrophobic drug (silymarin, β-carotene, or butylated hydroxyltoluene) dissolved in a suitable solvent (acetone or acetone/THF) and the receiver solution was pH 7.4 phosphate-buffered saline (PBS) and 0.5% wt/wt Pluronic F68.

Ten milliliter of the feed solution was filled into one half of the U-tube and 10 mL of the receiver solution was filled into the other half. A pressure of ~2 psi was applied to the feed solution tube using a compressed air outlet, which drives the feed solution through the nanoporous membrane. The nanoparticles were directly collected into a beaker with vigorous magnetic stirring to prevent nanoparticle aggregation. The nanoparticles were then filtered, rinsed 3 times using deionized water, and air dried at room temperature. The dried nanoparticles were evaluated for particle size and morphology using SEM. The nanoparticles were spherical in shape with average diameters of 75 ± 27 nm (silymarin), 102 ± 23 nm (β-carotene), and 130 ± 30 nm (butylated hydroxyltoluene). The size of these nanoparticles was smaller than the outer diameter of the nanoporous membrane (200 nm). This variation could be due to instantaneous precipitation of feed solution droplets and the strong wall shear force afforded by magnetic stirring, causing the nanoparticles to detach rapidly from the nanopore exits after solidification, preventing their continued growth. The particle size measurement for silymarin, β-carotene, and butylated hydroxyltoluene by DLS resulted in average diameters of 83, 105, and 132 nm, with polydispersity indices of 0.18, 0.238, and 0.234, respectively.

The solid-state form was evaluated using PXRD. All 3 model drugs displayed a halo pattern in PXRD, following NME confirming their amorphous nature. Dissolution was investigated using pH 5.5 and 7.4 PBS. After 8 h, 90% of the silymarin amorphous nanoparticles were dissolved, compared to 25% of silymarin crystalline powder. The greater dissolution profile of the nanoparticles was attributed to the increased surface area and the amorphous nature. Dissolution velocity of butylated hydroxyltoluene nanoparticles was faster compared to the untreated powder at pH 7.4 PBS buffer; however, at pH 5.5 the dissolution velocity for both forms was almost the same. The dissolution of β-carotene was not investigated.[69]

A list of methods and physicochemical parameters involved in the preparation and characterization of pharmaceutical amorphous nanoparticles is provided in Table 4.

Summary

This review article provides an exhaustive discussion of the mechanisms of preparation of amorphous nanoparticles along with a summary of techniques involved to analyze these novel drug delivery systems. A wide range of case studies are reported which describe the advantages of amorphous nanoparticles compared to macroamorphous and nanocrystalline formulations with respect to dissolution and the enhancement of oral bioavailability of BCS Class II and II/IV drugs. Amorphous nanoparticles are a relatively straightforward formulation strategy for the development of BCS Class II and II/IV drugs.

References

1. Lipinski C. Poor aqueous solubility—an industry wide problem in drug discovery. *Am Pharm Rev*. 2002;5(3):82-85.
2. Lipinski CA, Lombardo F, Dominy BW, Feeney PJ. Experimental and computational approaches to estimate solubility and permeability in drug discovery and development settings. *Adv Drug Deliv Rev*. 2012;64:4-17.
3. Lipinski CA. Drug-like properties and the causes of poor solubility and poor permeability. *J Pharmacol Toxicol Methods*. 2000;44(1):235-249.
4. Gribbon P, Andreas S. High-throughput drug discovery: what can we expect from HTS? *Drug Discov Today*. 2005;10(1):17-22.
5. Hann MM, Oprea TI. Pursuing the leadlikeness concept in pharmaceutical research. *Curr Opin Chem Biol*. 2004;8(3):255-263.
6. Yamashita S. *In vitro-in vivo* correlations: application to water insoluble drugs. *Bull Tech Gattefosse*. 1998:25-32.
7. Caldwell GW, Ritchie DM, Masucci JA, Hageman W, Yan Z. The new pre-preclinical paradigm: compound optimization in early and late phase drug discovery. *Curr Top Med Chem*. 2001;1(5):353-366.
8. Prentis RA, Lis Y, Walker SR. Pharmaceutical innovation by the seven UK-owned pharmaceutical companies (1964-985). *Br J Clin Pharmacol*. 1988;25(3):387-396.
9. Hartmann T, Schmitt J, Rohring C, Nimptsch D, Noller J, Mohr C. ADME related profiling in 96 and 384 well plate format—a novel and robust HT-assay for the determination of lipophilicity and serum albumin binding. *Curr Drug Deliv*. 2006;3(2):181-192.
10. Verma S, Huey BD, Burgess DJ. Scanning probe microscopy method for nanosuspension stabilizer selection. *Langmuir*. 2009;25(21):12481-12487.
11. Merisko-Liversidge E, Liversidge GG, Cooper ER. Nanosizing: a formulation approach for poorly-water-soluble compounds. *Eur J Pharm Sci*. 2003;18(2):113-120.
12. Merisko-Liversidge EM, Liversidge GG. Drug nanoparticles: formulating poorly water-soluble compounds. *Toxicol Pathol*. 2008;36(1):43-48.
13. Thomson W. On the equilibrium of vapour at a curved surface of liquid. *Proc R Soc Edinb*. 1872;7:63-68.
14. Van Eerdenbrugh B, Vermant J, Martens JA, et al. Solubility increases associated with crystalline drug nanoparticles: methodologies and significance. *Mol Pharm*. 2010;7(5):1858-1870.
15. Chiou WL, Riegelman S. Oral absorption of griseofulvin in dogs: increased absorption viasolid dispersion in polyethylene glycol 6000. *J Pharm Sci*. 1970;59(7):937-942.
16. Hancock BC, Parks M. What is the true solubility advantage for amorphous pharmaceuticals? *Pharm Res*. 2000;17(4):397-404.
17. Leuner C, Dressman J. Improving drug solubility for oral delivery using solid dispersions. *Eur J Pharm Biopharm*. 2000;50(1):47-60.
18. Serajuddin A. Solid dispersion of poorly water-soluble drugs: early promises, subsequent problems, and recent breakthroughs. *J Pharm Sci*. 1999;88(10):1058-1066.
19. Chen X, Young TJ, Sarkari M, Williams RO, Johnston KP. Preparation of cyclosporine A nanoparticles by evaporative precipitation into aqueous solution. *Int J Pharm*. 2002;242(1):3-14.
20. Lindfors L, Skantze P, Skantze U, Rasmusson M, Zackrisson A, Olsson U. Amorphous drug nanosuspensions. 1. Inhibition of Ostwald ripening. *Langmuir*. 2006;22(3):906-910.
21. Zhang JY, Shen ZG, Zhong J, et al. Preparation of amorphous cefuroxime axetil nanoparticles by controlled nanoprecipitation method without surfactants. *Int J Pharm*. 2006;323(1):153-160.
22. Wang JX, Zhang QX, Zhou Y, Shao L, Chen JF. Microfluidic synthesis of amorphous cefuroxime axetil nanoparticles with size-dependent and enhanced dissolution rate. *Chem Eng J*. 2010;162(2):844-851.
23. Zhu WZ, Wang JX, Shao L, Zhang HX, Zhang QX, Chen JF. Liquid antisolvent preparation of amorphous cefuroxime axetil nanoparticles in a tube-in-tube microchannel reactor. *Int J Pharm*. 2010;395(1):260-265.
24. Waard de H, Frijlink HW, Hinrichs WLJ. Bottom-up preparation techniques for nanocrystals of lipophilic drugs. *Pharm Res*. 2011;28(5):1220-1223.
25. Pace SN, Pace GW, Parikh I, Mishra AK. Novel injectable formulations of insoluble drugs. *Pharm Technol*. 1999;23(3):116-134.
26. Young TJ, Mawson S, Johnston KP, Henriksen IB, Pace GW, Mishra AK. Rapid expansion from supercritical to aqueous solution to produce submicron suspensions of water-insoluble drugs. *Biotechnol Prog*. 2000;16(3):402-407.
27. Heng D, Lee SH, Ng WK, Tan RBH. The nano spray dryer B-90. *Expert Opin Drug Deliv*. 2011;8(7):965-972.
28. Xie J, Lim LK, Phua Y, Hua J, Wang C-H. Electrohydrodynamic atomization for biodegradable polymeric particle production. *J Colloid Interf Sci*. 2006;302(1):103-112.
29. Zhang S, Kawakami K, Yamamoto M, et al. Coaxial electrospray formulations for improving oral absorption of a poorly water-soluble drug. *Mol Pharm*. 2011;8(3):807-813.
30. Ravichandran R. Nanoparticles in drug delivery: potential green nano-biomedicine applications. *Int J Nanotechnol Biomed*. 2009;1(2):B108-B130.

31. Nekkanti V, Pillai R, Vabalaboina V. *Drug Nanoparticles—An Overview*. Rijeka, Croatia: INTECH Open Access Publisher; 2012.
32. Patravale VB, Kulkarni RM. Nanosuspensions: a promising drug delivery strategy. *J Pharm Pharmacol*. 2004;56(7):827-840.
33. Junghanns JUAH, Muller RH. Nanocrystal technology, drug delivery and clinical applications. *Int J Nanomed*. 2008;3(3):295.
34. Kumar S, Burgess DJ. Nanosuspensions. In: Wright JC, Burgess DJ, eds. *Long Acting Injections and Implants*. New York, NY: Springer; 2012:239-261.
35. Loh ZH, Samanta AK, Heng PWS. Overview of milling techniques for improving the solubility of poorly water-soluble drugs. *Asian J Pharm Sci*. 2015;10(4):255-274.
36. Juhnke M, Weichert R. Nanoparticles of soft materials by high-energy milling at low temperatures. In: *7th World Congress of Chemical Engineering*. Germany; 2005.
37. Xie Y, Cho J, Kim S, Park K. Nanotechnology in drug delivery. In: Xie Y, ed. *The Nanobiotechnology Handbook*. Boca Raton, FL: CRC Press; 2013:519-534.
38. Morales JO, Watts AB, McConville JT. Mechanical particle-size reduction techniques. In: Williams RO, Watts AB, Miller DA, eds. *Formulating Poorly Water Soluble Drugs*. London: Springer; 2012:133-170.
39. Kumar A, Chen F, Mozhi A, et al. Innovative pharmaceutical development based on unique properties of nanoscale delivery formulation. *Nanoscale*. 2013;5(18):8307-8325.
40. Salazar J, Muller RH, Moschwitzer JP. Combinative particle size reduction technologies for the production of drug nanocrystals. *J Pharm*. 2014;2014(2014):1-15.
41. Gruverman IJ, Thumm JR. Production of nanostructures under ultra-turbulent collision reaction conditions—application to catalysts, superconductors, CMP abrasives, ceramics, and other nanoparticles. *MRS Proc*. 2003;P9:7.
42. Panagiotou T, Mesite S, Fisher R, Gruverman I. *Production of stable drug nanospensions using microfluidics reaction technology*. Proceedings of the NSTI Nanotechnology Conference and Trade Show. Santa Clara, CA: 2007:246-249.
43. Liversidge GG, Cundy KC. Particle size reduction for improvement of oral bioavailability of hydrophobic drugs: I. Absolute oral bioavailability of nanocrystalline danazol in beagle dogs. *Int J Pharm*. 1995;125(1):91-97.
44. Pilcer G, Sebti T, Amighi K. Formulation and characterization of lipid-coated tobramycin particles for dry powder inhalation. *Pharm Res*. 2006;23(5):931-940.
45. Huang Y, Dai WG. Fundamental aspects of solid dispersion technology for poorly soluble drugs. *Acta Pharm Sin B*. 2014;4(1):18-25.
46. Vaka SRK, Bommana MM, Desai D, Djordjevic J, Phuapradit W, Shah N. Excipients for amorphous solid dispersions. In: Shah N, Sandhu H, Choi DS, Choksi H, Malick W, eds. *Amorphous Solid Dispersions*. New York, NY: Springer; 2014:123-161.
47. Baghel S, Cathcart H, O'Reilly NJ. Polymeric amorphous solid dispersions: a review of amorphization, crystallization, stabilization, solid-state characterization, and aqueous solubilization of biopharmaceutical classification system class II drugs. *J Pharm Sci*. 2016;105(9):2527-2544.
48. Gulsun T, Gursoy RN, Levent O. Nanocrystal technology for oral delivery of poorly water-soluble drugs. *FARAD J Pharm Sci*. 2009;34:55-65.
49. Moschwitzer JP. Drug nanocrystals in the commercial pharmaceutical development process. *Int J Pharm*. 2013;453(1):142-156.
50. Junyaprasert VB, Morakul B. Nanocrystals for enhancement of oral bioavailability of poorly water-soluble drugs. *Asian J Pharm Sci*. 2015;10(1):13-23.
51. Lee J. Drug nano- and microparticles processed into solid dosage forms: physical properties. *J Pharm Sci*. 2003;92(10):2057-2068.
52. Van Eerdenbrugh B, Froyen L, Van Humbeeck J, Martens JA, Augustijns P, Van den Mooter G. Drying of crystalline drug nanosuspensions—the importance of surface hydrophobicity on dissolution behavior upon redispersion. *Eur J Pharm Sci*. 2008;35(1):127-135.
53. *Solid solutions and dispersions*3. Bethlehem, PA: Particle Sciences, Drug Development Services; 2012.
54. Amstad E, Gopinadhan M, Holtze C, et al. Production of amorphous nanoparticles by supersonic spray-drying with a microfluidic nebulator. *Science*. 2015;349(6251):956-960.
55. Rainer HM, Junghanns AH. Drug nanocrsytals/nanosuspensions for the delivery of poorly soluble drugs. In: Torchilin VP, ed. *Nanoparticulates as Drug Carriers*. London: Imperial College Press; 2006.
56. Bellantone RA. Fundamentals of amorphous systems: thermodynamic aspects. In: Shah N, Sandhu H, Choi DS, Choksi H, Malick W, eds. *Amorphous Solid Dispersions*. New York, NY: Springer; 2014:3-34.
57. Suslick KS. Sonochemistry. *Science*. 1990;247:1439-1445.
58. Thunemann AF. Polyelectrolyte-surfactant complexes (synthesis, structure and materials aspects). *Prog Polym Sci*. 2002;27(8):1473-1572.
59. Desgouilles SP, Vauthier C, Bazile D, et al. The design of nanoparticles obtained by solvent evaporation: a comprehensive study. *Langmuir*. 2003;19(22):9504-9510.
60. Dillen K, Vandervoort J, Van den Mooter G, Verheyden L, Ludwig A. Factorial design, physicochemical characterisation and activity of ciprofloxacin-PLGA nanoparticles. *Int J Pharm*. 2004;275(1):171-187.
61. Ramos L, Schonhoff M, Luan Y, Mohwald H, Brezesinski G. Electrostatic interactions between polyelectrolyte and amphiphiles in two-and three-dimensional systems. *Colloids Surf A Physicochem Eng Aspects*. 2007;303(1):79-88.
62. Taylor DJF, Thomas RK, Penfold J. Polymer/surfactant interactions at the air/water interface. *Adv Colloid Interface Sci*. 2007;132(2):69-110.
63. Dhumal RS, Biradar SV, Yamamura S, Paradkar AR, York P. Preparation of amorphous cefuroxime axetil nanoparticles by sonoprecipitation for enhancement of bioavailability. *Eur J Pharm Biopharm*. 2008;70(1):109-115.
64. Matteucci ME, Paguio JC, Miller MA, Williams Iii RO, Johnston KP. Flocculated amorphous nanoparticles for highly supersaturated solutions. *Pharm Res*. 2008;25(11):2477-2487.
65. Chi NT, Triet NM, Chien DM. Preparation of drug nanoparticles by emulsion evaporation method. *J Phys Conf Ser*. 2009;187:012047.
66. Zhu Z, Margulis-Goshen K, Magdassi S, Talmon Y, Macosko CW. Polyelectrolyte stabilized drug nanoparticles *via* flash nanoprecipitation: a model study with beta-carotene. *J Pharm Sci*. 2010;99(10):4295-4306.
67. Zeiger BW, Suslick KS. Sonofragmentation of molecular crystals. *J Am Chem Soc*. 2011;133(37):14530-14533.
68. Cheow WS, Hadinoto K. Self-assembled amorphous drug-polyelectrolyte nanoparticle complex with enhanced dissolution rate and saturation solubility. *J Colloid Interface Sci*. 2012;367(1):518-526.
69. Guo P, Hsu TM, Zhao Y, Martin CR, Zare RN. Preparing amorphous hydrophobic drug nanoparticles by nanoporous membrane extrusion. *Nanomedicine*. 2013;8(3):333-341.
70. Lonare AA, Patel SR. Antisolvent crystallization of poorly water soluble drugs. *Int J Chem Eng Appl*. 2013;4(5):337.
71. Cheow WS, Kiew TY, Yang Y, Hadinoto K. Amorphization strategy affects the stability and supersaturation profile of amorphous drug nanoparticles. *Mol Pharm*. 2014;11(5):1611-1620.
72. Homayouni A, Sadeghi F, Varshosaz J, Garekani HA, Nokhodchi A. Promising dissolution enhancement effect of soluplus on crystallized celecoxib obtained through antisolvent precipitation and high pressure homogenization techniques. *Colloids Surf B Biointerfaces*. 2014;122:591-600.
73. Zu Y, Sun W, Zhao X, et al. Preparation and characterization of amorphous amphotericin B nanoparticles for oral administration through liquid antisolvent precipitation. *Eur J Pharm Sci*. 2014;53:109-117.
74. Wijesena RN, Tissera N, Kannangara YY, Lin Y, Amaratunga GAJ, de Silva KMN. A method for top down preparation of chitosan nanoparticles and nanofibers. *Carbohydr Polym*. 2015;117:731-738.
75. Dizaj SM, Vazifehasl Z, Salatin S, Adibkia K, Javadzadeh Y. Nanosizing of drugs: effect on dissolution rate. *Res Pharm Sci*. 2015;10(2):95.
76. Montes A, Pereyra C, de la Ossa EJM, Gordillo MD. *Particles Formation Using Supercritical Fluids*. Rijeka, Croatia: INTECH Open Access Publisher; 2011.
77. Sheth P, Sandhu H. Amorphous solid dispersion using supercritical fluid technology. In: *Amorphous Solid Dispersions*. New York: Springer; 2014:579-591.
78. Lack E, Weidner E, Knez Z, Gruner S, Weinreich B, Seidlitz H. *Particle Generation with Supercritical CO_2*. Austria: Natex; 2005.
79. Yoshida VMH, Balcao VM, Vila MMDC, et al. Supercritical fluid and pharmaceutical applications. Part I: process classification. *Afr J Pharm Pharmacol*. 2016;10(9):132-144.
80. Rowe JM, Johnston KP. Precipitation technologies for nanoparticle production. In: Williams III RO, Watts AB, Miller DA, eds. *Formulating Poorly Water Soluble Drugs*. New York, NY: Springer; 2012:501-568.
81. Qian KK, Bogner RH. Application of mesoporous silicon dioxide and silicate in oral amorphous drug delivery systems. *J Pharm Sci*. 2012;101(2):444-463.
82. Liberman A, Mendez N, Trogler WC, Kummel AC. Synthesis and surface functionalization of silica nanoparticles for nanomedicine. *Surf Sci Rep*. 2014;69(2):132-158.
83. Petushkov A, Ndiege N, Salem AK, Larsen SC. Toxicity of silica nanomaterials: zeolites, mesoporous silica, and amorphous silica nanoparticles. *Adv Mol Toxicol*. 2010;4:223-266.
84. Bharti C, Nagaich U, Pal AK, Gulati N. Mesoporous silica nanoparticles in target drug delivery system: a review. *Int J Pharm Investig*. 2015;5(3):124.
85. Zhang H, Dunphy DR, Jiang X, et al. Processing pathway dependence of amorphous silica nanoparticle toxicity: colloidal vs pyrolytic. *J Am Chem Soc*. 2012;134(38):15790-15804.
86. Tarn D, Ashley CE, Xue M, Carnes EC, Zink JI, Brinker CJ. Mesoporous silica nanoparticle nanocarriers: biofunctionality and biocompatibility. *Acc Chem Res*. 2013;46(3):792-801.
87. Yu DG, Zhu LM, White K, Branford-White C. Electrospun nanofiber-based drug delivery systems. *Health*. 2009;1(02):67.
88. Ignatious F, Sun L, Lee CP, Baldoni J. Electrospun nanofibers in oral drug delivery. *Pharm Res*. 2010;27(4):576-588.
89. Verreck G, Chun I, Peeters J, Rosenblatt J, Brewster ME. Preparation and characterization of nanofibers containing amorphous drug dispersions generated by electrostatic spinning. *Pharm Res*. 2003;20(5):810-817.
90. Thassu D, Deleers M, Pathak YV. *Nanoparticulate Drug Delivery Systems*. Boca Raton, FL: CRC Press; 2007.
91. Haghi AK, Thomas S, Pourhashemi A, Hamrang A, Klodzinska E. *Nanomaterials and Nanotechnology for Composites: Design, Simulation and Applications*. Boca Raton, FL: CRC Press; 2015.
92. Cheow WS, Kiew TY, Hadinoto K. Amorphous nanodrugs prepared by complexation with polysaccharides: carrageenan versus dextran sulfate. *Carbohydr Polym*. 2015;117:549-558.
93. Jog R, Kumar S, Shen J, et al. Formulation design and evaluation of amorphous ABT-102 nanoparticles. *Int J Pharm*. 2016;498(1):153-169.

94. Kumar S, Shen J, Burgess DJ. Nano-amorphous spray dried powder to improve oral bioavailability of itraconazole. *J Control Release*. 2014;192:95-102.
95. Yang W, Johnston KP, Williams RO. Comparison of bioavailability of amorphous versus crystalline itraconazole nanoparticles *via* pulmonary administration in rats. *Eur J Pharm Biopharm*. 2010;75(1):33-41.
96. Matteucci ME, Brettmann BK, Rogers TL, Elder EJ, Williams Iii RO, Johnston KP. Design of potent amorphous drug nanoparticles for rapid generation of highly supersaturated media. *Mol Pharm*. 2007;4(5):782-793.
97. Kho K, Hadinoto K. Dry powder inhaler delivery of amorphous drug nanoparticles: effects of the lactose carrier particle shape and size. *Powder Technol*. 2013;233:303-311.
98. Smitha KT, Anitha A, Furuike T, Tamura H, Nair SV, Jayakumar R. *In vitro* evaluation of paclitaxel loaded amorphous chitin nanoparticles for colon cancer drug delivery. *Colloids Surf B Biointerfaces*. 2013;104:245-253.
99. Liu Y, Sun C, Hao Y, Jiang T, Zheng L, Wang S. Mechanism of dissolution enhancement and bioavailability of poorly water soluble celecoxib by preparing stable amorphous nanoparticles. *J Pharm Pharm Sci*. 2010;13(4):589-606.
100. Papadimitriou S, Bikiaris D. Novel self-assembled core-shell nanoparticles based on crystalline amorphous moieties of aliphatic copolyesters for efficient controlled drug release. *J Control Release*. 2009;138(2):177-184.
101. Thadkala K, Nanam PK, Rambabu B, Sailu C, Aukunuru J. Preparation and characterization of amorphous ezetimibe nanosuspensions intended for enhancement of oral bioavailability. *Int J Pharm Investig*. 2014;4(3):131.
102. Kim MS, Jin SJ, Kim J-S, et al. Preparation, characterization and *in vivo* evaluation of amorphous atorvastatin calcium nanoparticles using supercritical antisolvent (SAS) process. *Eur J Pharm Biopharm*. 2008;69(2):454-465.
103. Yu L, Li C, Le Y, Chen JF, Zou H. Stabilized amorphous glibenclamide nanoparticles by high-gravity technique. *Mater Chem Phys*. 2011;130(1):361-366.
104. Tran TTD, Tran PHL, Nguyen MNU, et al. Amorphous isradipine nanosuspension by the sonoprecipitation method. *Int J Pharm*. 2014;474(1):146-150.
105. Romero GB, Arntjen A, Keck CM, Muller RH. Amorphous cyclosporin A nanoparticles for enhanced dermal bioavailability. *Int J Pharm*. 2016;498(1):217-224.
106. Baig MS, Ahad A, Aslam M, Imam SS, Aqil M, Ali A. Application of Box-Behnken design for preparation of levofloxacin-loaded stearic acid solid lipid nanoparticles for ocular delivery: optimization, *in vitro* release, ocular tolerance, and antibacterial activity. *Int J Biol Macromol*. 2016;85:258-270.
107. Parikh T, Sandhu HK, Talele TT, Serajuddin ATM. Characterization of solid dispersion of itraconazole prepared by solubilization in concentrated aqueous solutions of weak organic acids and drying. *Pharm Res*. 2016;33(6):1456-1471.
108. Nguyen MH, Tran T-T, Hadinoto K. Controlling the burst release of amorphous drug-polysaccharide nanoparticle complex via crosslinking of the polysaccharide chains. *Eur J Pharm Biopharm*. 2016;104:156-163.
109. Li J, Wang H, Yang B, et al. Control-release microcapsule of famotidine loaded biomimetic synthesized mesoporous silica nanoparticles: controlled release effect and enhanced stomach adhesion in vitro. *Mater Sci Eng C Mater Biol Appl*. 2016;58:273-277.
110. Dalmolin LF, Khalil NM, Mainardes RM. Delivery of vanillin by poly (lactic-acid) nanoparticles: development, characterization and *in vitro* evaluation of antioxidant activity. *Mater Sci Eng C Mater Biol Appl*. 2016;62:1-8.
111. Ngwuluka NC, Kotak DJ, Devarajan PV. Design and characterization of metformin-loaded solid lipid nanoparticles for colon cancer. *AAPS Pharm Sci Tech*. 2016;17:1-11.
112. Huang PH, Hu SCS, Lee CW, Yeh AC, Tseng CH, Yen FL. Design of acid-responsive polymeric nanoparticles for 7, 3′, 4′-trihydroxyisoflavone topical administration. *Int J Nanomed*. 2016;11:1615.
113. Chonkar AD, Rao JV, Managuli RS, et al. Development of fast dissolving oral films containing lercanidipine HCl nanoparticles in semicrystalline polymeric matrix for enhanced dissolution and *ex vivo* permeation. *Eur J Pharm Biopharm*. 2016;103:179-191.
114. Suto B, Berko S, Kozma G, et al. Development of ibuprofen-loaded nanostructured lipid carrier-based gels: characterization and investigation of *in vitro* and *in vivo* penetration through the skin. *Int J Nanomed*. 2016;11:1201.
115. Burapapadh K, Takeuchi H, Sriamornsak P. Development of pectin nanoparticles through mechanical homogenization for dissolution enhancement of itraconazole. *Asian J Pharm Sci*. 2016;11(3):365-375.
116. Omwoyo WN, Melariri P, Gathirwa JW, et al. Development, characterization and antimalarial efficacy of dihydroartemisinin loaded solid lipid nanoparticles. *Nanomedicine*. 2016;12(3):801-809.
117. Zhu D, Tao W, Zhang H, et al. Docetaxel (DTX)-loaded polydopamine-modified TPGS-PLA nanoparticles as a targeted drug delivery system for the treatment of liver cancer. *Acta Biomater*. 2016;30:144-154.
118. Shi A, Li D, Liu H, Adhikari B, Wang Q. Effect of drying and loading methods on the release behavior of ciprofloxacin from starch nanoparticles. *Int J Biol Macromol*. 2016;87:55-61.
119. Parhizkar M, Reardon PJT, Knowles JC, et al. Electrohydrodynamic encapsulation of cisplatin in poly (lactic-co-glycolic acid) nanoparticles for controlled drug delivery. *Nanomedicine*. 2016;12(7):1919-1929.
120. Ghanbarzadeh S, Hariri R, Kouhsoltani M, Shokri J, Javadzadeh Y, Hamishehkar H. Enhanced stability and dermal delivery of hydroquinone using solid lipid nanoparticles. *Colloids Surf B Biointerfaces*. 2015;136:1004-1010.
121. Akl MA, Kartal-Hodzic A, Oksanen T, et al. Factorial design formulation optimization and in vitro characterization of curcumin-loaded PLGA nanoparticles for colon delivery. *J Drug Deliv Sci Technol*. 2016;32:10-20.
122. Gajra B, Patel RR, Dalwadi C. Formulation, optimization and characterization of cationic polymeric nanoparticles of mast cell stabilizing agent using the Box-Behnken experimental design. *Drug Dev Ind Pharm*. 2016;42(5):747-757.
123. Yang YC, Cai J, Yin J, Zhang J, Wang K-L, Zhang ZT. Heparin-functionalized Pluronic nanoparticles to enhance the antitumor efficacy of sorafenib in gastric cancers. *Carbohydr Polym*. 2016;136:782-790.
124. Maulvi FA, Lakdawala DH, Shaikh AA, et al. *In vitro* and *in vivo* evaluation of novel implantation technology in hydrogel contact lenses for controlled drug delivery. *J Control Release*. 2016;226:47-56.
125. Bhattacharya P, Mondal S, Basak S, Das P, Saha A, Bera T. *In vitro* susceptibilities of wild and drug resistant *Leishmania donovani* amastigotes to piperolactam A loaded hydroxypropyl-beta-cyclodextrin nanoparticles. *Acta Trop*. 2016;158:97-106.
126. Mostafa AA, Zaazou MH, Chow LC, et al. Injectable nanoamorphous calcium phosphate based in situ gel systems for the treatment of periapical lesions. *Biomed Mater*. 2015;10(6):065006.
127. Geetha P, Sivaram AJ, Jayakumar R, Mohan CG. Integration of in silico modeling, prediction by binding energy and experimental approach to study the amorphous chitin nanocarriers for cancer drug delivery. *Carbohydr Polym*. 2016;142:240-249.
128. Abd-Elrahman AA, El Nabarawi MA, Hassan DH, Taha AA. Ketoprofen mesoporous silica nanoparticles SBA-15 hard gelatin capsules: preparation and *in vitro*/*in vivo* characterization. *Drug Deliv*. 2016;23:1-29.
129. Tadros MI, Al-mahallawi AM. Long-circulating lipoprotein-mimic nanoparticles for smart intravenous delivery of a practically-insoluble antineoplastic drug: development, preliminary safety evaluations and preclinical pharmacokinetic studies. *Int J Pharm*. 2015;493(1):439-450.
130. Harmon P, Galipeau K, Xu W, Brown C, Wuelfing WP. Mechanism of dissolution-induced nanoparticle formation from a copovidone-based amorphous solid dispersion. *Mol Pharm*. 2016;13(5):1467-1481.
131. Jafari S, Maleki-Dizaji N, Barar J, Barzegar-Jalali M, Rameshrad M, Adibkia K. Methylprednisolone acetate-loaded hydroxyapatite nanoparticles as a potential drug delivery system for treatment of rheumatoid arthritis: in vitro and in vivo evaluations. *Eur J Pharm Sci*. 2016;91:225-235.
132. Maged A, Mahmoud AA, Ghorab MM. Nano-spray drying technique as a novel approach to formulate stable econazole nitrate nanosuspension formulations for ocular use. *Mol Pharm*. 2016;13:2951-2965.
133. Ji P, Yu T, Liu Y, et al. Naringenin-loaded solid lipid nanoparticles: preparation, controlled delivery, cellular uptake, and pulmonary pharmacokinetics. *Drug Des Dev Ther*. 2016;10:911-925.
134. Krull SM, Susarla R, Afolabi A, et al. Polymer strip films as a robust, surfactant-free platform for delivery of BCS Class II drug nanoparticles. *Int J Pharm*. 2015;489(1-2):45-57.
135. Badran MM, Harisa GI, AlQahtani SA, Alanazi FK, Zoheir KMA. Pravastatin-loaded chitosan nanoparticles: formulation, characterization and cytotoxicity studies. *J Drug Deliv Sci Technol*. 2016;32:1-9.
136. Najafi SHM, Baghaie M, Ashori A. Preparation and characterization of acetylated starch nanoparticles as drug carrier: ciprofloxacin as a model. *Int J Biol Macromol*. 2016;87:48-54.
137. Facchi SP, Scariot DB, Bueno PVA, et al. Preparation and cytotoxicity of N-modified chitosan nanoparticles applied in curcumin delivery. *Int J Biol Macromol*. 2016;87:237-245.
138. Zhang P, Liu X, Hu W, Bai Y, Zhang L. Preparation and evaluation of naringenin-loaded sulfobutylether-beta-cyclodextrin/chitosan nanoparticles for ocular drug delivery. *Carbohydr Polym*. 2016;149:224-230.
139. Su YR, Yu SH, Chao AC, et al. Preparation and properties of pH-responsive, self-assembled colloidal nanoparticles from guanidine-containing polypeptide and chitosan for antibiotic delivery. *Colloids Surfaces A Physicochem Eng Aspects*. 2016;494:9-20.
140. Zhang ZB, Xie ML, Kuang YY, et al. Preparation of amorphous drug nanoparticles by high-gravity reactive precipitation technique. *Chem Eng Process Process Intensif*. 2016;104:253-261.
141. Lingling G, Yuan Z, Weigen L. Preparation, optimization, characterization and in vivo pharmacokinetic study of asiatic acid tromethamine salt-loaded solid lipid nanoparticles. *Drug Dev Ind Pharm*. 2016;42(8):1-9.
142. Mazuryk J, Deptula T, Polchi A, et al. Rapamycin-loaded solid lipid nanoparticles: morphology and impact of the drug loading on the phase transition between lipid polymorphs. *Colloids Surfaces A Physicochem Eng Aspects*. 2016;502:54-65.
143. Fong SYK, Ibisogly A, Bauer-Brandl A. Solubility enhancement of BCS Class II drug by solid phospholipid dispersions: spray drying versus freeze-drying. *Int J Pharm*. 2015;496(2):382-391.
144. Siafaka P, Betsiou M, Tsolou A, et al. Synthesis of folate-pegylated polyester nanoparticles encapsulating ixabepilone for targeting folate receptor overexpressing breast cancer cells. *J Mater Sci Mater Med*. 2015;26(12):1-14.

145. Ayadi F, Bayer IS, Marras S, Athanassiou A. Synthesis of water dispersed nanoparticles from different polysaccharides and their application in drug release. *Carbohydr Polym*. 2016;136:282-291.
146. El-Naggar ME, El-Rafie MH, El-Sheikh MA, El-Feky GS, Hebeish A. Synthesis, characterization, release kinetics and toxicity profile of drug-loaded starch nanoparticles. *Int J Biol Macromol*. 2015;81:718-729.
147. Meng DL, Shang L, Feng XH, Huang XF, Che X. Xanthoceraside hollow gold nanoparticles, green pharmaceutics preparation for poorly water-soluble natural anti-AD medicine. *Int J Pharm*. 2016;506(1):184-190.
148. Karavas E, Georgarakis E, Bikiaris D. Felodipine nanodispersions as active core for predictable pulsatile chronotherapeutics using PVP/HPMC blends as coating layer. *Int J Pharm*. 2006;313(1):189-197.
149. Varshosaz J, Hassanzadeh F, Mahmoudzadeh M, Sadeghi A. Preparation of cefuroxime axetil nanoparticles by rapid expansion of supercritical fluid technology. *Powder Technol*. 2009;189(1):97-102.
150. Thakur R, Gupta RB. Formation of phenytoin nanoparticles using rapid expansion of supercritical solution with solid cosolvent (RESS-SC) process. *Int J Pharm*. 2006;308(1):190-199.
151. Thakur R, Gupta RB. Rapid expansion of supercritical solution with solid cosolvent (RESS-SC) process: formation of griseofulvin nanoparticles. *Ind Eng Chem Res*. 2005;44(19):7380-7387.
152. Gadermann M, Kular S, Al-Marzouqi AH, Signorell R. Formation of naproxen-polylactic acid nanoparticles from supercritical solutions and their characterization in the aerosol phase. *Phys Chem Chem Phys*. 2009;11(36):7861-7868.
153. Tandya A, Dehghani F, Foster NR. Micronization of cyclosporine using dense gas techniques. *J Supercrit Fluids*. 2006;37(3):272-278.
154. Ha ES, Kim JS, Baek IH, Hwang SJ, Kim MS. Enhancement of dissolution and bioavailability of ezetimibe by amorphous solid dispersion nanoparticles fabricated using supercritical antisolvent process. *J Pharm Investigation*. 2015;45(7):641-649.
155. Cardoso MAT, Monteiro GA, Cardoso JP, et al. Supercritical antisolvent micronization of minocycline hydrochloride. *J Supercrit Fluids*. 2008;44(2):238-244.
156. Adami R, Reverchon E, Jarvenpa E, Huopalahti R. Supercritical antisolvent micronization of nalmefene HCl on laboratory and pilot scale. *Powder Technol*. 2008;182(1):105-112.
157. Montes A, Bendel A, Kurti R, Gordillo MD, Pereyra C, de La Ossa EJM. Processing naproxen with supercritical CO_2. *J Supercrit Fluids*. 2013;75:21-29.
158. Kalogiannis CG, Pavlidou E, Panayiotou CG. Production of amoxicillin microparticles by supercritical antisolvent precipitation. *Ind Eng Chem Res*. 2005;44(24):9339-9346.
159. Reverchon E, Della Porta G, Falivene MG. Process parameters and morphology in amoxicillin micro and submicro particles generation by supercritical antisolvent precipitation. *J Supercrit Fluids*. 2000;17(3):239-248.
160. Reverchon E, De Marco I, Caputo G, Della Porta G. Pilot scale micronization of amoxicillin by supercritical antisolvent precipitation. *J Supercrit Fluids*. 2003;26(1):1-7.
161. Tenorio A, Gordillo MD, Pereyra C, de la Ossa EJM. Controlled submicro particle formation of ampicillin by supercritical antisolvent precipitation. *J Supercrit Fluids*. 2007;40(2):308-316.
162. Thakur R, Gupta RB. Production of hydrocortisone micro-and nano-particles using supercritical anti-solvent with enhanced mass transfer. *Chem Eng Commun*. 2006;193(3):293-305.
163. Reverchon E, De Marco I, Della Porta G. Rifampicin microparticles production by supercritical antisolvent precipitation. *Int J Pharm*. 2002;243(1):83-91.
164. Zhao X, Zu Y, Jiang R, et al. Preparation and physicochemical properties of 10-hydroxycamptothecin (HCPT) nanoparticles by supercritical antisolvent (SAS) process. *Int J Mol Sci*. 2011;12(4):2678-2691.
165. Kim JS, Kim MS, Park HJ, Jin SJ, Lee S, Hwang SJ. Physicochemical properties and oral bioavailability of amorphous atorvastatin hemi-calcium using spray-drying and SAS process. *Int J Pharm*. 2008;359(1):211-219.
166. Thiering R, Dehghani F, Dillow A, Foster NR. The influence of operating conditions on the dense gas precipitation of model proteins. *J Chem Technol Biotechnol*. 2000;75(1):29-41.
167. Thiering R, Dehghani F, Dillow A, Foster NR. Solvent effects on the controlled dense gas precipitation of model proteins. *J Chem Technol Biotechnol*. 2000;75(1):42-53.
168. Muhrer G, Mazzotti M. Precipitation of lysozyme nanoparticles from dimethyl sulfoxide using carbon dioxide as antisolvent. *Biotechnol Prog*. 2003;19(2):549-556.
169. Kuang YY, Zhang ZB, Xie ML, Wang JX, Le Y, Chen JF. Large-scale preparation of amorphous cefixime nanoparticles by antisolvent precipitation in a high-gravity rotating packed bed. *Ind Eng Chem Res*. 2015;54(33):8157-8165.
170. Mohseni M, Gilani K, Mortazavi SA. Preparation and characterization of rifampin loaded mesoporous silica nanoparticles as a potential system for pulmonary drug delivery. *Iran J Pharm Res*. 2015;14(1):27-34.
171. Vadia N, Rajput S. Study on formulation variables of methotrexate loaded mesoporous MCM-41 nanoparticles for dissolution enhancement. *Eur J Pharm Sci*. 2012;45(1):8-18.
172. Thomas MJK, Slipper I, Walunj A, et al. Inclusion of poorly soluble drugs in highly ordered mesoporous silica nanoparticles. *Int J Pharm*. 2010;387(1):272-277.
173. Zhang Y, Zhi Z, Jiang T, Zhang J, Wang Z, Wang S. Spherical mesoporous silica nanoparticles for loading and release of the poorly water-soluble drug telmisartan. *J Control Release*. 2010;145(3):257-263.
174. Wani A, Muthuswamy E, Savithra GHL, Mao G, Brock S, Oupicky D. Surface functionalization of mesoporous silica nanoparticles controls loading and release behavior of mitoxantrone. *Pharm Res*. 2012;29(9):2407-2418.
175. Qian W, Yu DG, Li Y, Liao YZ, Wang X, Wang L. Dual drug release electrospun core-shell nanofibers with tunable dose in the second phase. *Int J Mol Sci*. 2014;15(1):774-786.
176. Natu MV, de Sousa HC, Gil MH. Effects of drug solubility, state and loading on controlled release in bicomponent electrospun fibers. *Int J Pharm*. 2010;397(1):50-58.
177. Tungprapa S, Jangchud I, Supaphol P. Release characteristics of four model drugs from drug-loaded electrospun cellulose acetate fiber mats. *Polymer*. 2007;48(17):5030-5041.
178. Verreck G, Chun I, Rosenblatt J, et al. Incorporation of drugs in an amorphous state into electrospun nanofibers composed of a water-insoluble, nonbiodegradable polymer. *J Control Release*. 2003;92(3):349-360.
179. Taepaiboon P, Rungsardthong U, Supaphol P. Drug-loaded electrospun mats of poly (vinyl alcohol) fibres and their release characteristics of four model drugs. *Nanotechnology*. 2006;17(9):2317.
180. Yu DG, Williams GR, Yang JH, Wang X, Qian W, Li Y. Chitosan nanoparticles self-assembled from electrospun composite nanofibers. *J Textile Sci Eng*. 2012;2012:1-5.
181. Xie J, Wang CH. Electrospun micro-and nanofibers for sustained delivery of paclitaxel to treat C6 glioma in vitro. *Pharm Res*. 2006;23(8):1817-1826.
182. Yu DG, Branford-White C, Shen XX, Zhang XF, Zhu LM. Solid dispersions of ketoprofen in drug-loaded electrospun nanofibers. *J Dispers Sci Tech*. 2010;31(7):902-908.
183. Li X, Kanjwal MA, Lin L, Chronakis IS. Electrospun polyvinyl-alcohol nanofibers as oral fast-dissolving delivery system of caffeine and riboflavin. *Colloids Surf B Biointerfaces*. 2013;103:182-188.
184. Illangakoon UE, Gill H, Shearman GC, et al. Fast dissolving paracetamol/caffeine nanofibers prepared by electrospinning. *Int J Pharm*. 2014;477(1):369-379.
185. Nagy ZK, Balogh A, Demuth B, et al. High speed electrospinning for scaled-up production of amorphous solid dispersion of itraconazole. *Int J Pharm*. 2015;480(1):137-142.
186. Kim K, Luu YK, Chang C, et al. Incorporation and controlled release of a hydrophilic antibiotic using poly (lactide-co-glycolide)-based electrospun nanofibrous scaffolds. *J Control Release*. 2004;98(1):47-56.
187. Yu DG, Yang JM, Branford-White C, Lu P, Zhang L, Zhu LM. Third generation solid dispersions of ferulic acid in electrospun composite nanofibers. *Int J Pharm*. 2010;400(1):158-164.
188. Yu DG, Gao LD, White K, Branford-White C, Lu WY, Zhu LM. Multicomponent amorphous nanofibers electrospun from hot aqueous solutions of a poorly soluble drug. *Pharm Res*. 2010;27(11):2466-2477.
189. Yu DG, Branford-White C, White K, Li XL, Zhu LM. Dissolution improvement of electrospun nanofiber-based solid dispersions for acetaminophen. *AAPS Pharm Sci Tech*. 2010;11(2):809-817.
190. Li XY, Wang X, Yu DG, et al. Electrospun borneol-PVP nanocomposites. *J Nanomater*. 2012;2012:7.
191. Nagy ZK, Balogh A, Vajna B, et al. Comparison of electrospun and extruded soluplus®-based solid dosage forms of improved dissolution. *J Pharm Sci*. 2012;101(1):322-332.
192. Vigh T, Horvathova T, Balogh A, et al. Polymer-free and polyvinylpirrolidone-based electrospun solid dosage forms for drug dissolution enhancement. *Eur J Pharm Sci*. 2013;49(4):595-602.
193. Sun XZ, Williams GR, Hou XX, Zhu LM. Electrospun curcumin-loaded fibers with potential biomedical applications. *Carbohydr Polym*. 2013;94(1):147-153.
194. Nagy ZK, Balogh A, Dravavolgyi G, et al. Solvent-free melt electrospinning for preparation of fast dissolving drug delivery system and comparison with solvent-based electrospun and melt extruded systems. *J Pharm Sci*. 2013;102(2):508-517.
195. Yu DG, Shen XX, Branford-White C, White K, Zhu LM, Bligh SWA. Oral fast-dissolving drug delivery membranes prepared from electrospun polyvinylpyrrolidone ultrafine fibers. *Nanotechnology*. 2009;20(5):055104.
196. Yu DG, Zhang XF, Shen XX, Brandford-White C, Zhu LM. Ultrafine ibuprofen-loaded polyvinylpyrrolidone fiber mats using electrospinning. *Polym Int*. 2009;58(9):1010-1013.
197. Shen X, Yu D, Zhu L, Branford-White C, White K, Chatterton NP. Electrospun diclofenac sodium loaded Eudragit® L 100-55 nanofibers for colon-targeted drug delivery. *Int J Pharm*. 2011;408(1):200-207.
198. Karthikeyan K, Guhathakarta S, Rajaram R, Korrapati PS. Electrospun zein/eudragit nanofibers based dual drug delivery system for the simultaneous delivery of aceclofenac and pantoprazole. *Int J Pharm*. 2012;438(1):117-122.